The Relationship Between US East Coast Sea Level and Large Scale North Atlantic Circulation

by
Wyn Pauly

A thesis submitted to the
Faculty and Honors Council of the
University of Colorado in partial fulfillment
of the requirements for honors for the degree of
Bachelors of Arts
Department of Atmospheric and Oceanic Sciences
2024

This thesis entitled:
The Relationship Between US East Coast Sea Level and Large Scale North Atlantic Circulation
written by Wyn Pauly
has been approved for the Department of Atmospheric and Oceanic Sciences

Prof. Kristopher Karnauskas (Atmospheric and Oceanic Sciences)

Prof. Derek Brown (Atmospheric and Oceanic Sciences)

Prof. Steven Nerem (Aerospace Engineering Sciences)

Date _____

The final copy of this thesis has been examined by the signatories, and we find that both the content and the form meet acceptable presentation standards of scholarly work in the above mentioned disciplines.

Abstract

The US East Coast is exceptionally vulnerable to changes in coastal sea level. Variability in basin scale dynamics drive changes in coastal sea level. This thesis works to quantify the relationship between these dynamics and coastal sea level to explain inter-annual tide gauge variability.

A range of tide gauge data, an ocean reanalysis product, an atmospheric retrospective state estimate, and a range of satellite based observational datasets are used throughout this thesis.

A correlation matrix was created to depict the relationship between tide gauges to the north and south of Cape Hatteras. Empirical Orthogonal Function (EOF) analysis is additionally conducted on the tide gauge data to explore how they move in connection to one another. This analysis revealed the Annual Split Mode (ASM) that drives the inverse relationship between tide gauges on either side of Cape Hatteras. The ASM, North Atlantic Oscillation (NAO) and Atlantic Meridional Mode (AMM) were then linearly regressed onto sea surface temperature (SST), sea surface height (SSH), sea level pressure (SLP) and wind stress fields to determine their basin scale expression. This analysis produced the North Atlantic Common Mode (NACM), defined as the shared component of variability between the NAO and AMM. EOF analysis was then conducted on ECCO SSH, barotropic streamfunction (SF), and wind stress fields. These EOFs revealed the dominant modes of variability that govern each field on interannual time scales. Finally, the ASM and NACM were linearly regressed onto these ECCO fields to quantify the contribution of the barotropic SF.

The tide gauge correlation matrix depicted an inverse relationship between the tide gauges to the north and to the south of Cape Hatteras. The ASM quantifies this relationship. Both the ASM and NACM produce regression coefficient maps that demonstrate a consistent SST and SSH tripole pattern associated with the strengthening or weakening of the westerlies and trade winds. The regression of these modes onto ECCO data highlighted the role of changes in gyre transport in generating the observed SSH tripole pattern. Finally, the NACM was found to be responsible for approximately 50% of the variance in the first ECCO EOF for barotropic SF and SSH, and up to 75% of the variance explained in the first wind EOF. It was also found to explain 52% of the ASM.

52% of the inverse relationship between the regions north and south of Cape Hatteras on annual time scales is explained by the NACM. These changes in sea level along the coast are a result of changes in basin scale dynamics. Additionally, these basin scale dynamics are driven by changes in prevailing wind stress patterns. This results in changes in turbulent heat flux that contribute to the SST tripole pattern, in addition to changes in barotropic SF that contribute to both the SST and SSH tripole patterns.

Wind-driven basin-scale dynamics across the entire North Atlantic drive changes in coastal sea level along the US East Coast. The effects of this interannual variability alternate sign across Cape Hatteras. The results of this thesis indicate that future changes in basin-scale dynamics can have spatially complex effects on coastal sea level.

Table Of Contents

1. Introduction

1.1 Background

The US East Coast is exceptionally vulnerable to changes in coastal sea level. Variability in basin scale dynamics drive changes in coastal sea level. This thesis works to quantify the relationship between these dynamics and coastal sea level to explain inter-annual tide gauge variability.

The ocean circulation in the North Atlantic basin is comprised of both density and wind driven components. The density driven component, AMOC, overlaps spatially with the subtropical and subpolar wind driven gyres. The culmination of these two components results in the circulation depicted in Figure 1. The time averaged state of the wind driven gyres are further explained in Section 1.4.

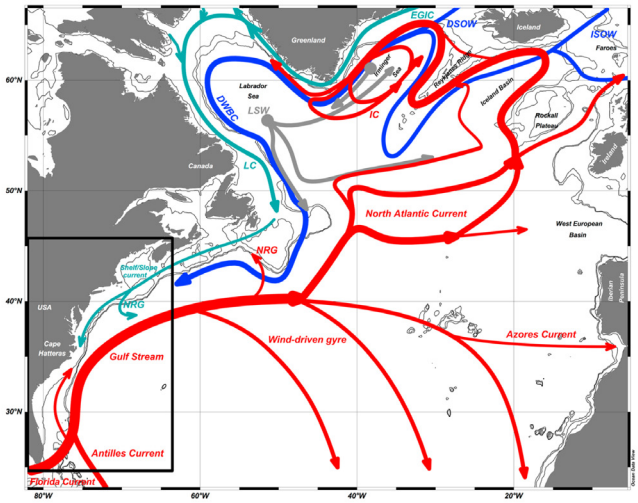

Figure 1 : Schematic of North Atlantic Circulation from Little et al., 2019

There are two primary modes of interannual variability that dominate the North Atlantic Region. The first mode is the North Atlantic Oscillation (NAO). This is defined as changes in sea level pressure (SLP) between the Iceland's and the Azores' regions (Walker, 1924). This results in changes in the prevailing winds in this region. This variability then further leads to changes in SST, among other variables. The second mode is the Atlantic Meridional Mode. This is defined as a meridional shifts in the Atlantic Intertropical Convergence Zone. This leads to SST, wind and various other anomalies in the tropical Atlantic.

This thesis explores the nature of interannual sea level variability at the coast, in addition to the role of these modes of climatic variability on coastal sea level. The following section will further explain other mechanisms that alter coastal sea level.

1.2 Known Causes of Sea Level Variability

There are a variety of oceanic, atmospheric and geophysical processes that affect sea level on local and regional scales. Figure 2 highlights a couple of these primary processes.

Vertical land motion is one of the primary confounds in tide gauge data. This motion is due to the lasting impact of the previous glacial period. Places where there were large land glaciers experienced a depression of the continental plates as a result of the increased mass loading. Due to the absence of these glaciers, the continental plates are rebounding to resume their initial vertical location. This results in the tide gauge itself moving relative

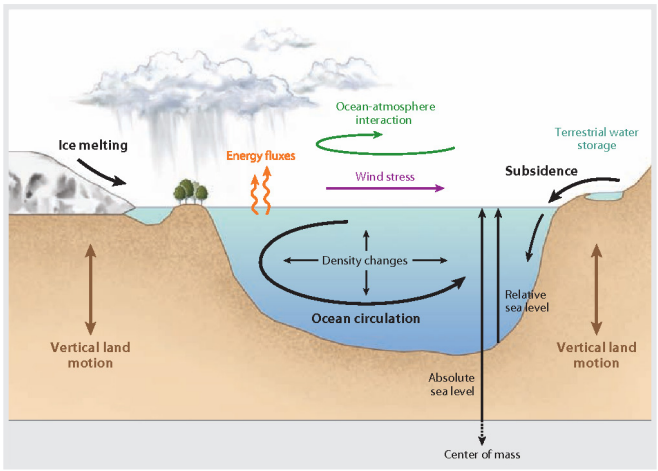

Figure 2 : Stammers et al., Causes for Contemporary Regional Sea Level Changes, Annual Review of Marine Science, 2013

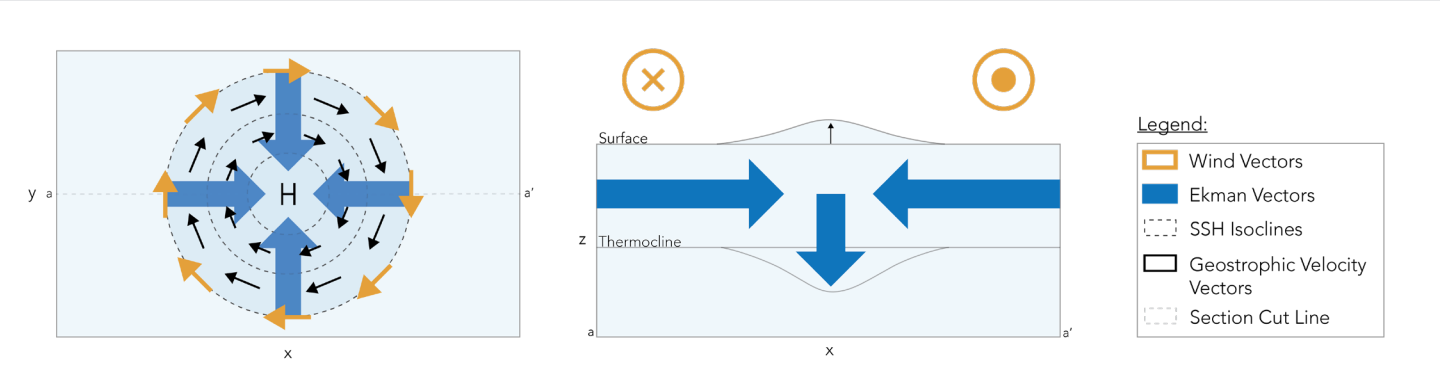

Figure 3 : Schematic Diagram of the processes involved in gyre formation and establishment of geostrophic flow

to the surface of the ocean.

The other primary process that is a confound in tide gauge data is the inverse barometer effect. This quantifies the impact of atmospheric surface pressure on sea level. In regions where there is a surface low, there is a slight increase in sea surface height due to the decrease in mass loading in the atmosphere. Both of these effects have been accounted for in the tide gauge and sea surface height data used in this thesis.

The processes that we are most interested in exploring are ocean circulation and wind stress. Wind stress along the surface of the ocean has a large impact on the direction in which the upper layers of the ocean move. This process is further explained in the following section. Ocean circulation, as mentioned in the previous section, is composed of both density driven and wind driven circulations. In this thesis we will primarily focus on the wind driven component, as it is more sensitive to interannual variability and atmosphere ocean interactions.

Wind driven circulation, outside of the tropics, is largely dominated by large-scale gyres. In the North Atlantic, the two large-scale gyres present are denoted as the subtropical gyre located in the mid latitudes, and the subpolar gyre located at higher latitudes. The physical mechanisms that drive gyre formation will be discussed in the following section.

1.3 Mechanistic Development of the Gyres

The wind-driven gyres are mechanistically driven by prevailing winds. Figure 3 is a schematic diagram that explains this formative process.

Initial wind stress along the ocean's surface in a circular shape initiates the entire process. This is an approximation of the prevailing wind pattern over the subtropics in the northern hemisphere. Due to the Coriolis force, wind stress along the surface of the ocean results in water movement 90 degrees to the right of the initial stress. In this scenario, these factors result in the convergence of water movement toward the center of the circular wind pattern. This convergence of water at the surface results in both a depression of the thermocline, and an increase in sea surface height at the center. The result is something that resembles a hill at the center of this wind stress pattern. This then creates a pressure gradient force toward the outside of the gyre. A balance between these divergent and convergent forces is then realized through geostrophic currents. These currents are considered to be in geostrophic balance precisely because they balance the pressure gradient force and Coriolis force. These geostrophic currents flow clockwise around the hill at the center, mimicking the initial pattern of wind stress. These currents are what we refer to as the wind-driven gyres.

These mechanisms also apply to the subpolar gyre. The primary difference between

the gyres in these two regions is the direction of initial wind stress. However, in the subpolar gyre region the initial wind stress is counterclockwise. This results in Ekman divergence, leading to a 'valley' and an elevation of the thermocline at the center of the gyre region.

It is important to note that this description is idealized without the effect of western intensification. The true shape and locations of these gyres, including western boundary currents, are pictured in Figure 4 and described in Section 1.4.

These wind driven gyres play a large role in ocean circulation. Due to the role of wind stress and SSH in their development, it is likely that they will have substantial interannual variability, in addition to driving variability in the SSH field.

Ekman Transport

The movement of water 90 degrees to the right of wind stress in the northern hemisphere, responsible for convergence at the center of the subtropical gyre, is referred to as Ekman transport. The Coriolis force does not drive the entire water column 90 degrees to the right. It actually affects the water column in a more nuanced way, through an Ekman spiral pictured in Figure 4.

The wind stress at the surface results in a shallow surface current that moves slightly to the right of the wind stress direction as it balances the Coriolis force and the forcing from above. The layer of water below this shallow surface layer then behaves the same way, balancing the stress from above. Except, in this case, the stress from above is from the surface current. This second layer then has an input stress that is already slightly to the right, and it proceeds to balance this stress with the Coriolis force, resulting in movement of water slightly further to the right than the surface layer. This process continues as you descend through the water column. The end result is the entire surface water column moving 90 degrees to the right of the initial wind stress.

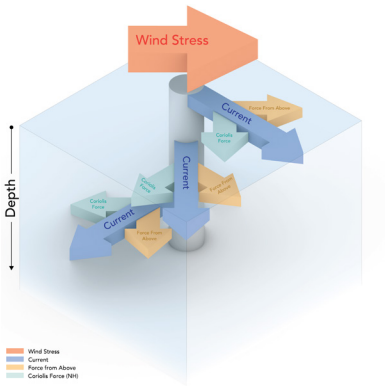

Figure 4 : Schematic Diagram of an Ekman Spiral

These dynamics are derived from the equations of motion under steady state conditions. As such, they occur on seasonal and longer time scales, as they are the ocean's steady state response to wind forcing.

Ekman transport can be described as the connection between atmospheric wind stress and ocean dynamics. Because Ekman transport is one of the main ways that wind stress generates water movement, it may be one the primary mechanisms that drives sea surface height variability at the coast. Throughout this thesis, we will investigate the interannual variability and anomalies of wind stress, streamfunction and sea surface height. To understand the context in which thee anomalies occur, the following 2 sections will describe the mean state of the streamfunction and wind stress fields.

1.4 Barotropic Streamfunction

The Barotropic Streamfunction is defined as the streamfunction calculated from the vertically integrated velocity field. ECCO velocity data is used to create the time-averaged barotropic SF plot shown in Figure 5.

This plot depicts the approximate shape and locations of the subtropical and subpolar gyre. The region in the mid latitudes associated with positive Sv values is the subtropical gyre. The black contour around this region is the +15 Sv contour. Similarly, the region in the high latitudes associated with negative Sv values is the subpolar gyre. The black contour around this region is the -15 Sv contour. These +/- 15 Sv contours will be used in subsequent maps as a reference frame for gyre location.

In comparison to Section 1.3, this

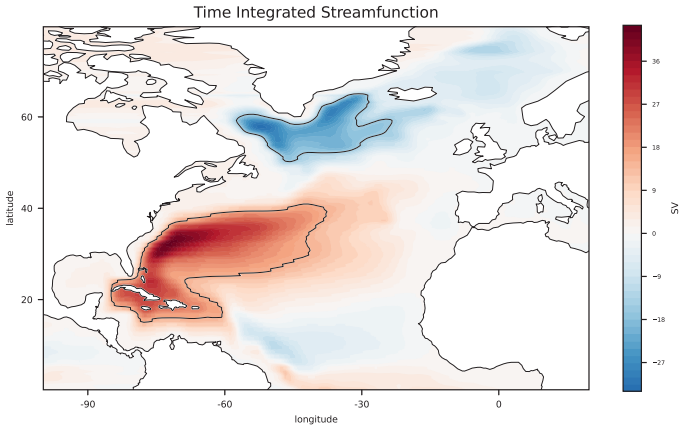

Figure 5 : Time Averaged Barotropic SF, black contours are located at +/- 15 Sv

representation of gyre circulation is more realistic. The unsymmetrical shape with respect to longitude is a result of western intensification. This is a result of the conservation of potential vorticity. Due to the fact that the angular momentum associated with earth's rotation increases with decreasing latitude, any given water parcel will begin to rotate to compensate. This results in water parcels along the western boundary of the subtropical gyre rotating counterclockwise to compensate for the decreasing planetary vorticity as they move northward. The result is an intense and narrow western boundary current, balanced by much slower and broader southward transport cross the majority of the Atlantic basin.

1.5 Prevailing Wind Patterns

The Prevailing Wind map shown in Figure 6 is generated by the time averaged wind stress field from ERA5.

The prevailing westerly winds between 40-65°N are the westerlies, and the prevailing north easterly winds between 10-30°N are the trade winds.

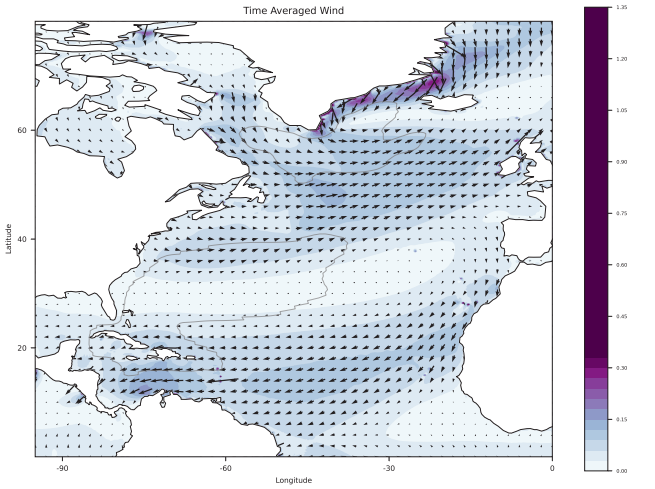

Figure 6 : Time Averaged Wind Stress field

1.6 Hypothesis

Wind stress plays a large role in both local and remote SSH variability. Wind stress is the driving force behind gyre development and associated transport. As such, we expect variability in the wind stress field to result in similar variability in gyre transport. We expect this variability to then drive changes in SSH on a basin scale. However, this variability in wind stress may also drive other processes such as changes in turbulent heat flux across the basin, or Ekman transport along the coast. We seek to understand the role of these remote and local processes in driving the observed sea level variability along the US East Coast.

2. Data and Methods

2.1 Tide Gauge Data

The Permanent Service for Mean Sea Level (PSMSL) serves as the data bank of global long-term tide gauge sea level information (Holgate et al., 2013). PSMSL acquires its data from over 2000 active tide gauges globally, analyzes the quality and spatial consistency of mean sea level data on monthly and annual time scales, and then distributes these time series to the scientific community. The subset of this data that is determined to be of research quality, is referenced as the Revised Local Reference (RLR) dataset. This data is defined as being consistent with a set of locally defined benchmarks through time.

The temporal duration of these data sets is variable. The average length of RLR data is 37 years, with the longest datasets associated with tide gauges located in the Northern Hemisphere, and particularly around Northern Europe. However there are a few exceptions located in North America, Asia and Australia.

Vertical land motion is the primary bias to recorded sea level in tide gauge records. Vertical land motion occurs on many temporal and spatial scales. The largest regional component is the slow continued response of the earth's crust to the after effects of the last ice age. The magnitude of this vertical movement is largely determined by the locations of glaciers during the previous ice age and can be larger than changes in sea level itself. The process of mitigating this signal is called glacial isostatic adjustment. The rates of vertical land motion are determined through the use of Earth model predictions and through Global Navigation Satellite System (GNSS) data. Other drivers of vertical land motion include tectonic events and anthropogenic subsidence resulting from extractive processes (such as ground water or oil). The augmentation of tide gauges with GNSS systems has increased in practice in recent years, making this control process more implicit.

The second primary bias to observed sea level in tide gauge records is the sea surface displacement associated with atmospheric pressure. This references the phenomena through which atmospheric pressure variability affects sea surface pressure resulting in the displacement of water. The correction for this phenomena is called the inverted barometer (IB) correction. This correction is particularly important for analyzing sea level over spatial and temporal time scales as atmospheric pressure loading varies both temporally and by latitude.

While the spatial coverage of in situ observations of RLR data have increased in recent years, there are still limitations presented by the spatial and temporal coverage of tide gauges. These limitations motivate the analysis of additional datasets in this thesis described below.

PSMSL data from 43 tide gauges along the US East Coast ranging in latitude from 25.73°N

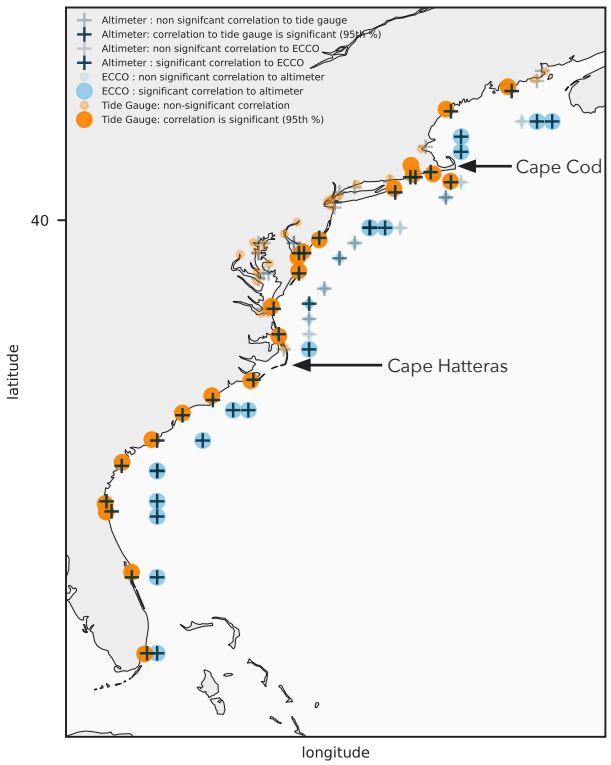

Figure 7 : Map of tide gauges and their relationship to nearest Altimeter data and ECCO data

to 44.9°N are analyzed in this thesis over a 25 year period of from 1992 to 2017. These tide gauges are shown in Figure 7. The region south of Cape Hatteras will be referred as the South Atlantic Bight (SAB). The region located between Cape Hatteras and Cape Cod will be referred to as the Mid Atlantic Bight (MAB). The region north of Cape Cod will be referred to as the Gulf of Maine (GOM).

These tide gauges are not uniformly distributed, and are not all located in regions that have direct connections to the open ocean. Thus, a subsample of these tide gauges was selected for analysis. From these 43 tide gauges, 22 were selected.

The first step in the selection process was to identify tide gauges that had a significant correlation with the nearest satellite altimeter grid cell. This correlation sheds light on the accuracy of the tide gauges, in addition to highlighting tide gauges that are too far inland. Locations too far inland are farther away from their nearest altimeter grid cell, which can result in nonsignificant correlations. Because of the nature of this thesis, it is imperative that the tide gauge data is influenced by basin scale processes.

The second selection process was to identify the nearest offshore ECCO grid cell. The sea surface height values at these 43 locations were then correlated to their nearest altimeter grid cell. This process allows us to identify regions off of the US East Coast that are not modeled well by ECCO. This revealed that some regions of the Mid-Atlantic Bight, in particular, are not well modeled.

The final step in this process was to correlate the altimeter data nearest to the tide gauges, to the altimeter data nearest to the ECCO grid cells. This step allows us to quantify the relationship between the data from coastal tide gauges to the open ocean.

The result of this process was the selection of 22 tide gauges that were both significantly correlated to the nearest altimeter grid cell, in addition to being significantly correlated to altimeter grid cell in the open ocean. For more information on this process, see Section 7.1.

Tide Gauge data is the basis of most of the analysis in this thesis. It is first used to understand the relationship between tide gauges located at different latitudes along the US East Coast. This is done through correlations as well as Singular Value Decomposition (SVD). This analysis involves decomposing a 2D or 3D dataset into orthogonal principal components (PCs). Each of these PCs have a spatial and temporal component in addition to a singular value that is related to the percent variance explained by that mode. The original signal of each mode can be obtained by multiplying the temporal component, the spatial component and the singular value. The complete signal can then be reconstructed by repeating this process for each PC and summing. SVD is the mathematical basis of Empirical Orthogonal Function (EOF) analysis. Thus, in the following sections, when this type of analysis is applied to data that varies in both space and time, it will be referred to as EOF analysis. This denotes the fact there are both a spatial and temporal component.

2.2 AMOC Data

RAPID MOC monitoring project provides a combination of in-situ observations and transport estimates from atmospheric reanalysis data to estimate the streamfunction of Atlantic Overturning Circulation (AMOC). The RAPID array consists of numerous moorings that measure temperature and salinity continuously at locations ranging from depths just below surface to the sea floor (https://rapid.ac.uk/background.php). Data from this array is available from April, 2004 through February of 2022 (Moat et al., 2022). A schematic diagram of the RAPID array is pictured in Figure 8.

The three component variables of AMOC are Ekman transport along 26.5°N, Florida Straights Transport, and the Upper Mid-Ocean Transport. The sum of these three components is represented by the variable MOC that represented the net overturning transport.

At depths ranging from 0-800 meters, the net mid-ocean flow is generally southward, while depths ranging from 800-1100 meters are typically dominated by northward flow. Upper mid-ocean transport is defined as the

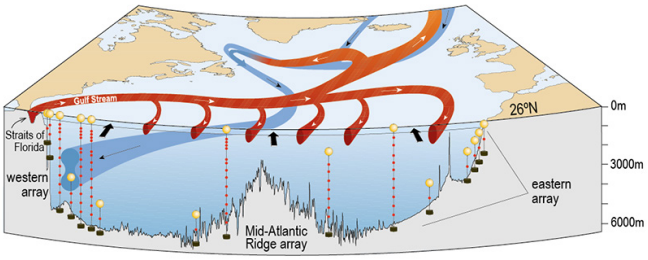

Figure 8 : Schematic Diagram of the Rapid Array from https://rapid.ac.uk/background.php

net flow above the depth at which the minimum value of southward mid-ocean transport occurs. This depth is defined at each time step by the separation of intermediate northward flow (above) and dominating southward flow (below). The upper mid-ocean time series is the integrated transport from the surface to this depth.

Florida Straights Transport is defined as the depth integrated flow between the West Palm Beach region of the Florida coast and the Grand Bahama Island. This is the region of ocean through which the Florida current flows before becoming part of the western boundary current known as the Gulf Stream. These values are collected based on electromagnetic cable measurements. Due to the conductive nature of the ocean and the consistent influence of earth's magnetic field, wherever water is in motion, electric potentials and currents will occur (Stommel, 1948). Thus, the measurement of voltage differences across these submarine telephone cables are used to infer the changes in water column transport (Baringer & Larsen, 2001).

The Ekman Transport time series is calculated from ERA5 wind stress data along the 26.5°N transect of the North Atlantic. ERA5 is one version of the ECMWF global climate atmospheric reanalysis dataset (https://registry.opendata.aws/ecmwf-era5/). This reanalysis is conducted by using ECMWF's Integrated Forecast System to process satellite and in-situ station data.

In this thesis, RAPID data will be used to analyze the relationships between the variables described above and local sea level along the US East Coast.

2.3 ECCO Data

The Estimating the Circulation and Climate of the Ocean (ECCO) dataset combines the MITgcm ocean circulation model with global ocean datasets to produce a data assimilated ocean model. ECCO is an adjoint model, which means that it is suited for assessing the sensitivity of model data differences from observations and investigating the internal dynamics of complex systems. Another benefit of adjoint modeling is the ability to study causation. Sensitivity can be used to quantify the contributions of different driving components of the ocean based on their modeled relationships (Fukumori, 2022). Because of these characteristics, ECCO data is useful for exploring the relationships between various oceanic processes.

ECCO is an ocean model that satisfies the laws of physics and thermodynamics, estimates temperature and salinity, 3D momentum, sea surface height, density, and precipitation in addition to providing estimates of the atmospheric state (https://ecco-group.org/data.htm). ECCO provides the ability to examine oceanic processes for which no in-situ observations are available, and is thus used in this thesis.

ECCO data provides the opportunity to explore the velocity fields of the entire North Atlantic Basin using the barotropic streamfunction (SF), in addition to SSH and wind stress. First, EOF analysis is conducted to explore the dominant modes of variability within these fields. Second, various time series associated with modes of variability are linearly regressed onto these same fields. This analysis provides an understanding of any differences between ECCO and observational data, in addition to gaining an understanding of the SF anomalies that accompany these modes of variability.

2.4 ERA5 Data

ERA5 is a global climate and weather reanalysis product from the European Centre for Medium-Range Weather Forecasts (ECMWF). This product uses a data assimilated

physics based model to produce global climate estimates.

This dataset will be used in this thesis for linear regressions. The linear regression will provide a visualization of basin scale wind stress and SLP patterns that are associated with various modes of variability.

2.5 NOAA OI SST V2

This dataset is a NOAA Physical Sciences Laboratory (PSL) product. It is a high resolution SST anomaly dataset produced through the use of multi-satellite sensor data. OI stands for optimum interpolation. This means that data collected from satellites, ships, buoys and Argo floats are interpolated into a regular grid. This provides the ability to confirm and correct sea level data across data collection methods, in addition to providing complete spatial coverage. The anomalies are then calculated by subtracting the 30-year climatological mean.

This dataset will be used in this thesis for linear regressions. The linear regression will provide a visualization of basin scale SST patterns that are associated with various modes of variability.

2.6 JPL MEaSUREs Gridded Sea Surface Height Anomalies

This dataset is a product of the NASA Jet Propulsion Laboratory. It is a high resolution SSH anomaly dataset derived through the combination of a myriad of satellite altimeter and advanced microwave radiometer datasets.

Similar to the NOAA OI SST dataset, this dataset will be used in this thesis for linear regressions. The linear regression will provide a visualization of basin scale SSH patterns associated with various modes of viability.

2.7 NAO and AMM Data

The North Atlantic Oscillation (NAO) and Atlantic meridional Mode (AMM) time series used throughout this thesis are a product of the NOAA PSL Climate Indices web page.

3. Analysis

3.1 Tide Gauge Relationships

This section describes the relationships between the 22 tide gauges located along the US East Coast . The first portion will examine their annually averaged correlations. The following sections will then describe the components of this relationship and seasonality through the use of SVD analysis.

Previous work (Diabaté et al., 2021) has identified an inverse correlation between the tide gauges on either side of the location at which the Gulf Stream detaches from the continental shelf. Throughout this thesis, this location will be referenced as Cape Hatteras.

We conducted a similar analysis and produced the correlation matrix in Figure 9. This matrix describes a strong and significant correlation between all of the tide gauges south of Cape Hatteras (upper left corner). This figure also describes a strong and significant correlation between the tide gauges north of Cape Hatteras (bottom right corner). The correlation values between these two regions are predominantly negative. The magnitude of the correlation values across regions are smaller than that of the correlation values within the same region. Despite their smaller magnitude, many of the negative correlation values between regions are still significant. This significance decreases as you approach the boundary at Cape Hatteras.

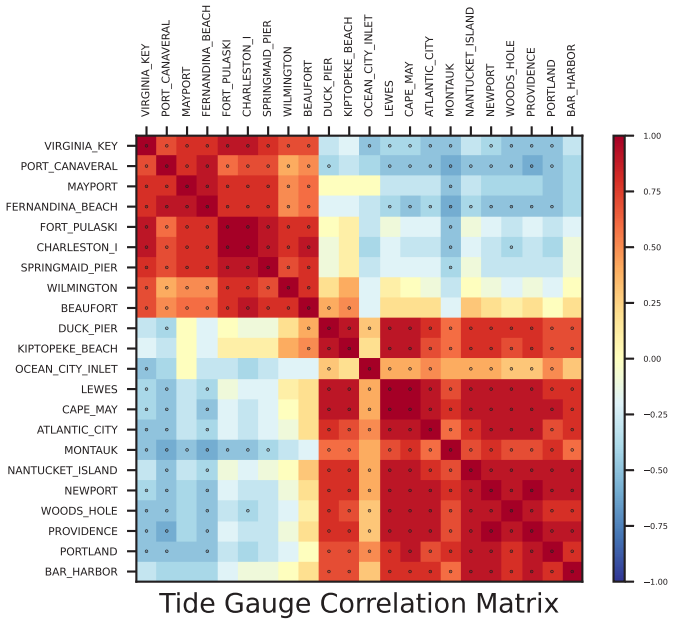

Figure 9 : Tide Gauge Correlation Matrix. The dots represent significance at the 95th percentile.

The next step in understanding the relationships between these tide gauges is to understand how they vary spatially and temporally. This is done through the use of EOF analysis.

3.1.1 Annual Tide EOF

SVD analysis was conducted on the annually averaged and detrended set of 22 tide gauge time series. This revealed two primary modes shown in Figure 10.

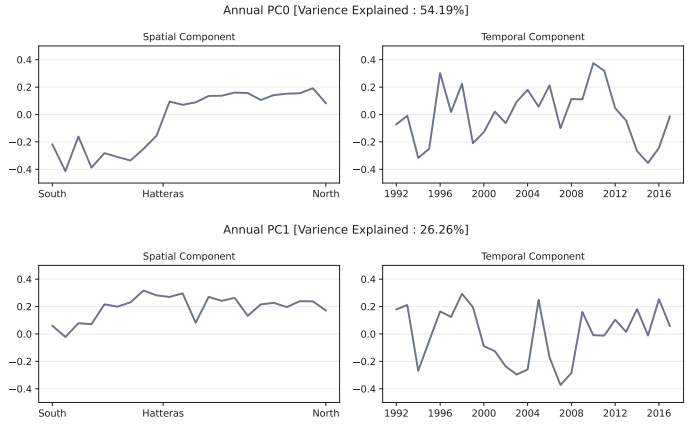

Figure 10 : Annual tide gauge PC0 and PC1. Left column shows the spatial component, while the right shows the time series.

The first mode represents a spatial split across Cape Hatteras. This indicates that the regions South and North of Cape Hatteras have inverse relationships with the SVD time series. This mode explains 54% of the variance in this dataset. As this analysis progresses, SVD modes that show a spatial split across Cape Hatteras will be referenced as 'Split Modes' and the one derived from annually averaged data will be

referred to as the annual split mode (ASM).

The second mode represents a predominantly uniform spatial relationship across the entire US East Coast to the associated time series. This indicates that the modes of variability captured in this SVD component drive similar changes in sea level down the entire coast. This mode explains 26% of the variance in this dataset. In the following analysis, modes that show similar expressions down the entire coast will be referenced as 'Homogeneous Modes.'

Using annually averaged data can potentially lead to averaging out signals and natural variability across seasons. Since the winter months, defined as December, January and February (DJF) in the northern hemisphere, are considered to be associated with increased activity in the climate system, this season is typically selected for analyzing interannual variability. However, in the following sections, we show that using annually averaged data is reasonable in this particular context through seasonal SVD analysis. Through this analysis we found that each season's variance is dominated by a homogeneous and split mode to varying degrees.

3.1.2 Seasonal Homogeneous Modes

For each season, EOF analysis yielded a homogeneous mode as the first principal component, with the exception of March, April May (MAM), for which it was the second mode. These spatial and temporal components are shown in Figure 11.

It is notable that the spatial component of each of these principal components (PC) look very similar. They each have a larger expression south of Cape Hatteras. While this similarity is interesting, temporally they are generally not significantly correlated. These correlation values are also shown in Figure 11.

These low significance values indicate that the sea level at the coast is driven uniformly by different modes of variability across seasons. Despite the large fractions of variance explained associated with these modes, due to their temporal differences it is reasonable that the annual homogeneous mode comprises a

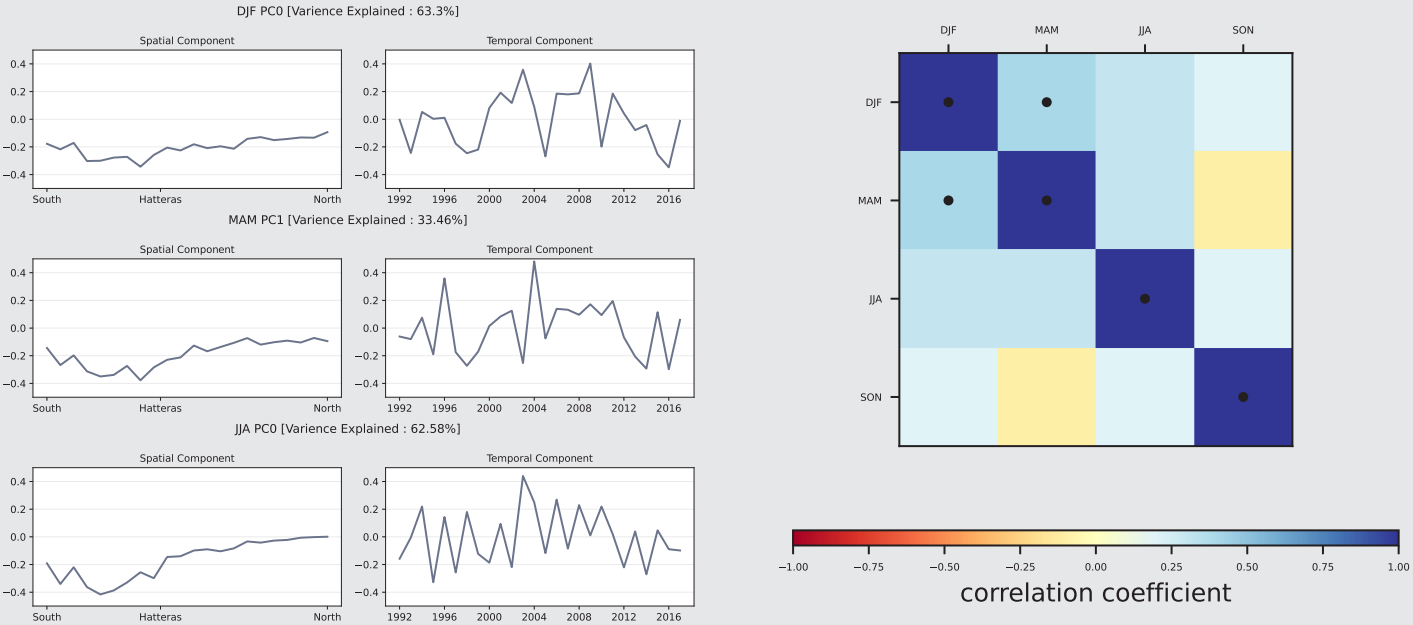

Figure 11 : Homogeneous SVD modes for each season (DJF, MAM, JJA, SON). Spatial components are in the left column, temporal on the right. Correlation between temporal components shown above. Dots signify significance at the 95th percentile. SON correlated to following DJF & MAM.

much lower fraction.

3.1.3 Seasonal Split Modes

For each season, EOF analysis yielded a split mode as the second principal component, with the exception of MAM, for which it was the first. These spatial and temporal components are shown in Figure 12.

All of these modes demonstrate very similar spatial behavior. For all of these modes, the region south of Cape Hatteras predominantly has a positive spatial coefficient. Similarly, the region north of Cape Hatteras has a predominantly negative spatial coefficient. Additionally, their temporal components are positively and significantly correlated. This indicates that there are similar modes of variability present within each of these PCs.

With the exception of MAM, the variance explained by these modes are relatively small, ranging from 19-30%. However, due to their strong correlation and overall similarity, we expect these modes to be maintained in annual averages. Thus, unlike the homogeneous mode, the split mode increases in variance explained when considering the annual average.

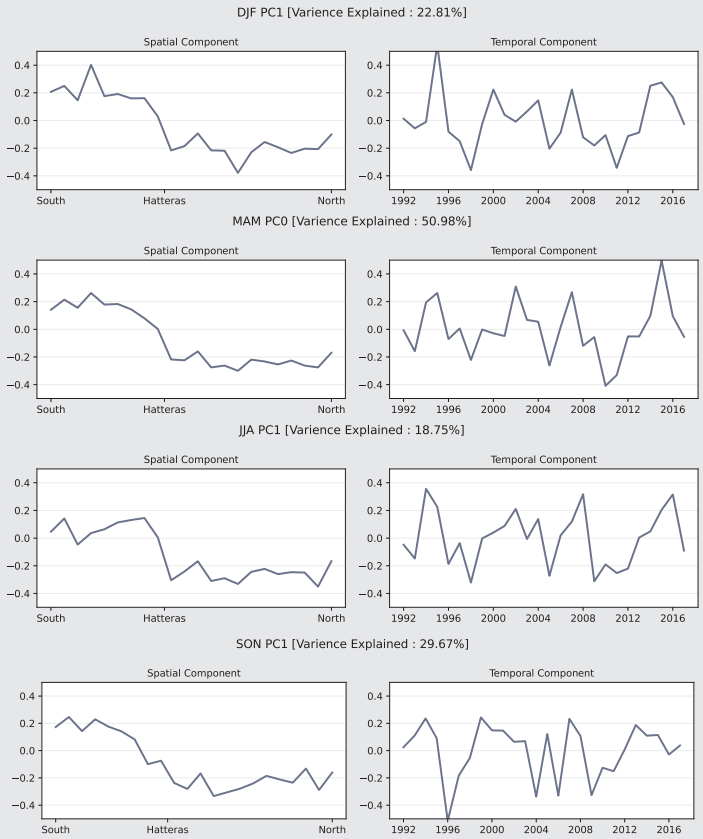

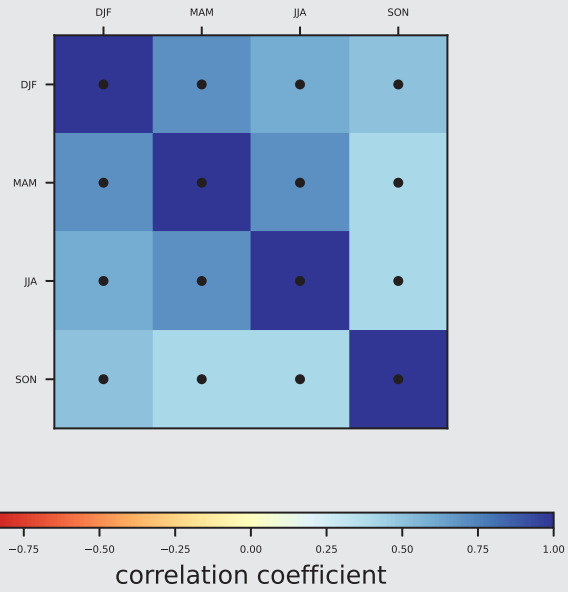

Figure 12 : Split SVD modes for each season (DJF, MAM, JJA, SON). Spatial components are in the left column, temporal on the right. Correlation between temporal components shown above. Dots signify significance at the 95th percentile. SON correlated to following DJF & MAM.

3.2 AMOC and Tide Gauge Correlation

From the Rapid Array dataset, the net overturning transport, the upper mid ocean transport, the Florida straights transport and the Ekman transport time series were analyzed. These time series are shown in Figure 13. The annual mean time series of each of the 22 tide gauges and the Rapid Array data were correlated. These values are shown in Figure 14.

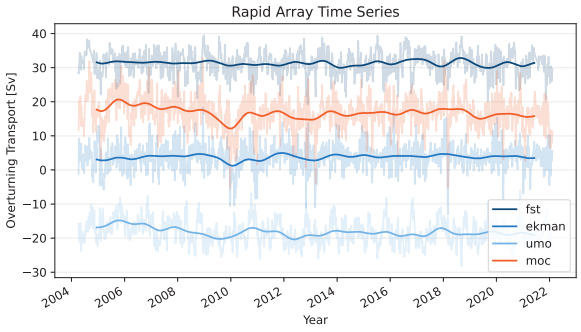

Figure 13 : Low Pass filtered RAPID Array Time Series. Florida Straights Transport (fst), Ekman Transport (ekman), Upper Mid Ocean (umo), Net Overturning Transport (moc)

From this analysis, we can see that the net overturning transport in the North Atlantic Basin is correlated to tide gauges along the US East Coast. It is interesting that we see a change in correlation sign between the tide gauges located on either side of Cape Hatteras. This indicates that when the net overturning transport in the North Atlantic Basin increases in magnitude, sea level in the SAB also increases. In contrast, sea level in the NAB and GOM decreases with increasing strength of transport. However none of these correlations are significant at the 95th percentile.

In the graph of correlation values for the density driven component of Atlantic circulation, referenced as the upper mid-ocean transport, we see very small correlation values. These very small values are consistent along the entire coast. This indicates that the split across Cape Hatteras is not related to the density driven component of the Atlantic large scale circulation.

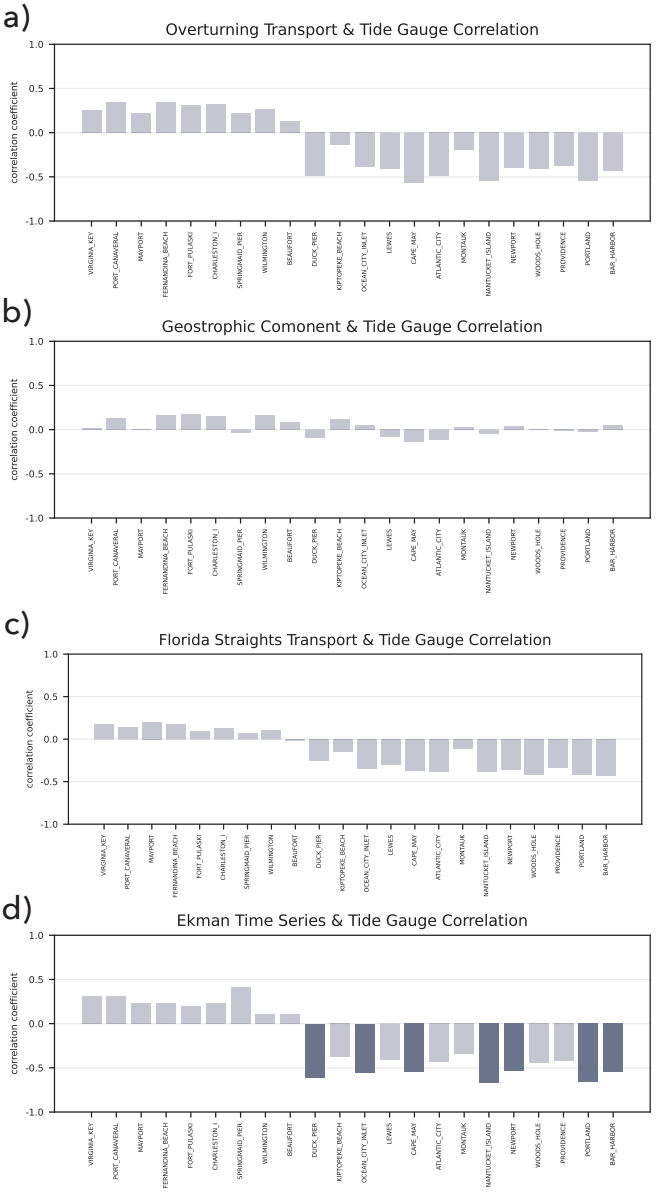

Figure 14 : Correlation Values between tide gauges and a) MOC b) Geostrophic Component (umo) c) Florida Straights Transport d) Ekman Transport

In the graph of correlation values for the headwaters of the Gulf Stream, referenced as Florida Straights transport, we see the same split across Cape Hatteras. While the correlation values in the SAB are relatively small, it is interesting that the NAB and GOM have a larger magnitude of anti-correlation. The Gulf Stream is the western boundary current of the subtropical gyre. This analysis is purely statistical in nature; mechanistic diagnosis is warranted (see Section 3.4).

In the graph of correlation values between the tide gauges and Ekman transport along 26.5°N, the SAB has positive correlation values, while the NAB and GOM have negative

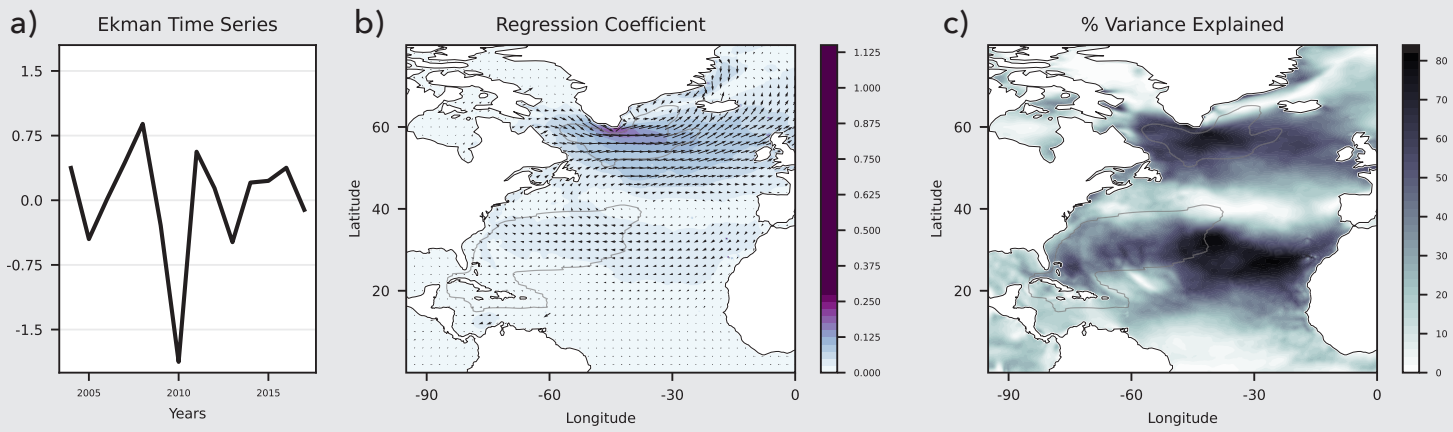

Figure 15 : a) Annually averaged Ekman Time Series b) Regression Coefficient, Grey lines correspond to +/- 15 Sv from the barotropic streamfunction c) Percent Variance Explained

correlation values. This variable has the largest and most significant correlation to the tide gauges. This is particularly interesting considering this variable only measures northward transport of water that results from zonal wind stress in one specific region of the North Atlantic. This indicates that these values of Ekman transport may be related to a larger scale pattern of wind stress and subsequent Ekman transport over the entire North Atlantic Basin.

This analysis highlighted the influence of wind stress over the North Atlantic Basin as one of the potential drivers of US East Coast sea level variability. In order to understand the structure of wind stress patterns we will examine ERA5 wind stress data in the following section.

3.2.1 Basin Scale Expression of the Ekman Transport Time Series

To examine the basin scale wind stress patterns associated with the Ekman Transport times series from the RAPID Array, ERA5 wind stress data is used to generate a regression map shown in Figure 15.

The wind vectors in this regression coefficient map are consistent with a strengthening of the westerlies, and trade winds over the Subpolar Atlantic and Mid-Atlantic, respectively. This accounts for a large amount of the overall variance in these regions as well. As we show later in this analysis, this wind stress pattern is consistent with the regression maps produced by the NAO and AMM.

3.3 Basin Scale Expressions of the ASM, NAO and AMM

Linear Regression Coefficient maps are used in this section to understand the basin scale expression of various time series. The following time series were normalized and then projected onto altimeter, SST, SLP and wind stress time series to produce a map of the linear regression coefficients. These maps are also accompanied by percent variance explained maps to quantify the contribution of the time series being regressed.

3.3.1 NAO vs AMM

The NAO and AMM are defined as two separate modes of variability driven by different mechanisms and located in different regions of the North Atlantic. It is also evident in the time series that the AMM acts on slower timescales, while the NAO is subject to more seasonal and interannual variability (Seip et al., 2019). Despite these differences, the regression maps of these two modes of variability, pictured in Figures 16 and 17, are remarkably similar. These two time series have a correlation value of -0.57 ($p = 0.002$), which explains the flip in regression coefficient signs.

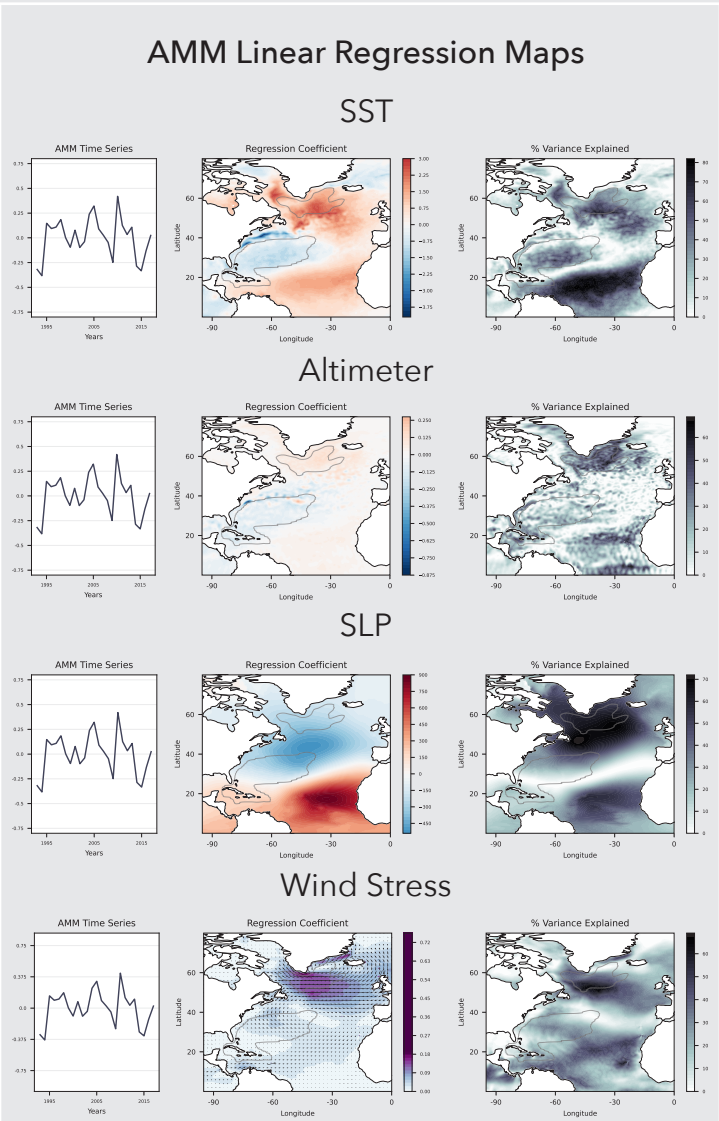

Figure 16 : AMM Regression Maps

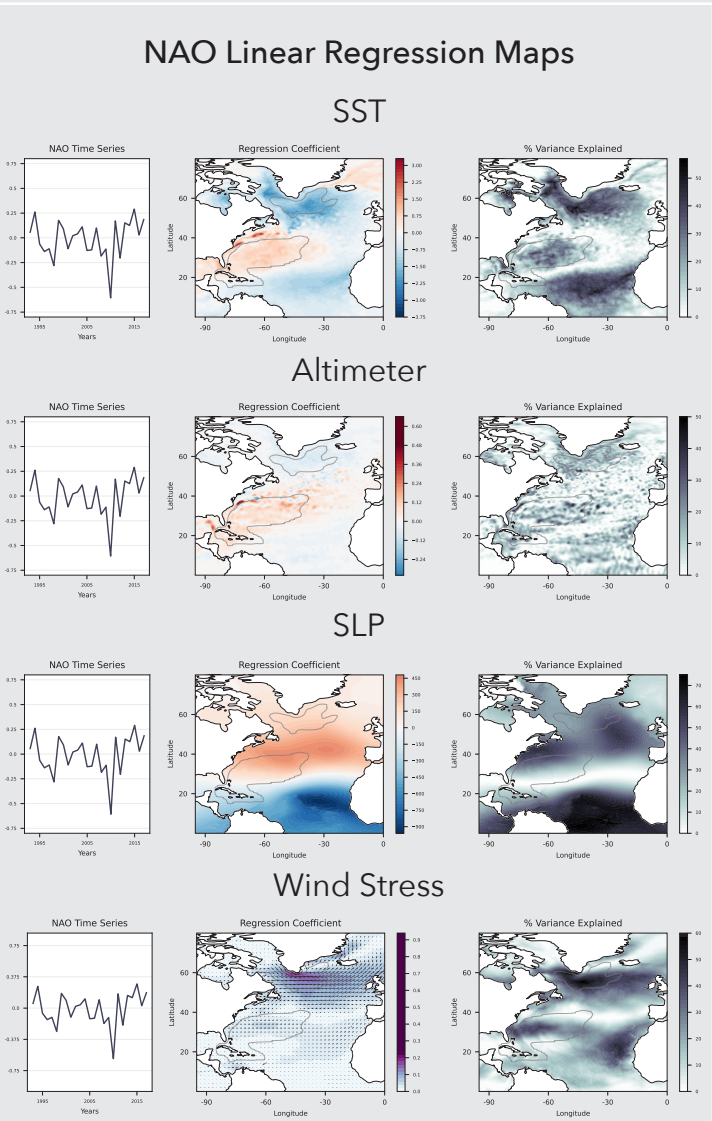

Figure 17 : NAO Regression Maps

Both of these modes of variability result in an SST tripole pattern. This tripole pattern is associated with the weakening (strengthening) of the westerlies and trade winds depicted in the wind stress regression coefficient map for the AMM (NAO). It is stated in previous work (Frankignoul 1985; Cayan 1992) that this SST tripole pattern, in part, is driven by changes in turbulent heat fluxes (THF) associated with the NAO. However, the similarities between the NAO and AMM linear regression coefficient maps indicates that this tripole may not be driven by the NAO alone.

Both of these modes also result in an SSH tripole pattern that mirrors the SST tripole pattern. The mechanism driving this SSH pattern is not directly related to changes in wind stress, but may be indirectly related through changes in the wind driven component of oceanic circulation.

While some small differences between these two modes of variability and the amount of variance they explain is evident in these linear regression maps, it is also evident that there is basin scale variability tied to both of these modes. While they may not share the same high frequency variability, they impact the North Atlantic Basin in very similar ways and at similar times. This indicates that they are two parts of a larger mode of variability that dominates the entire North Atlantic Basin. In the subsequent sections, the shared component of these two modes of variability will be identified and referred to as the North Atlantic Common Mode (NACM).

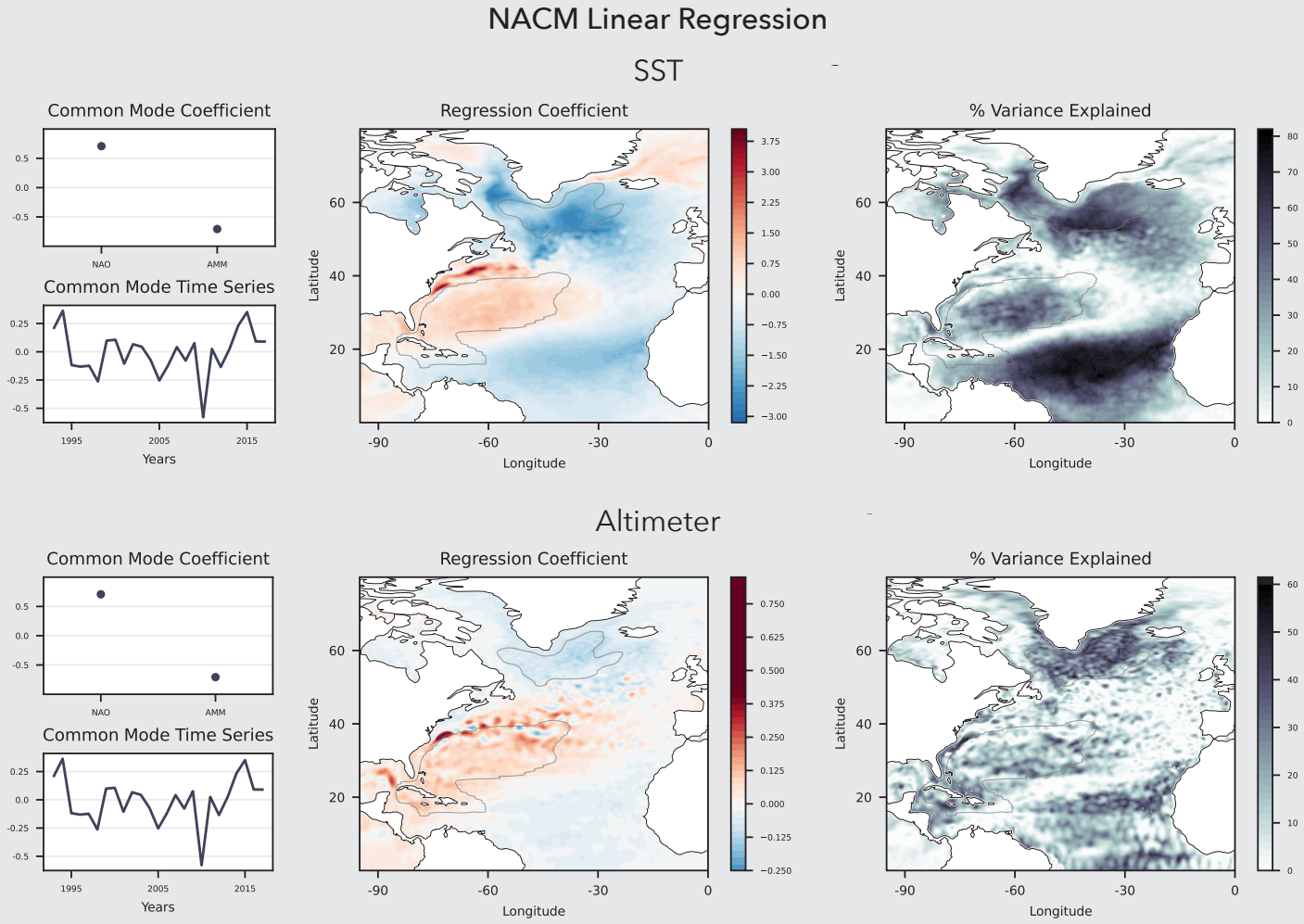

Figure 18 : Common Mode linear regression plots onto SST and Altimeter data. Spatial and temporal components of PC0 are in the left most column. Regression coefficient maps are in the center. Percent Variance explained is in the right most column.

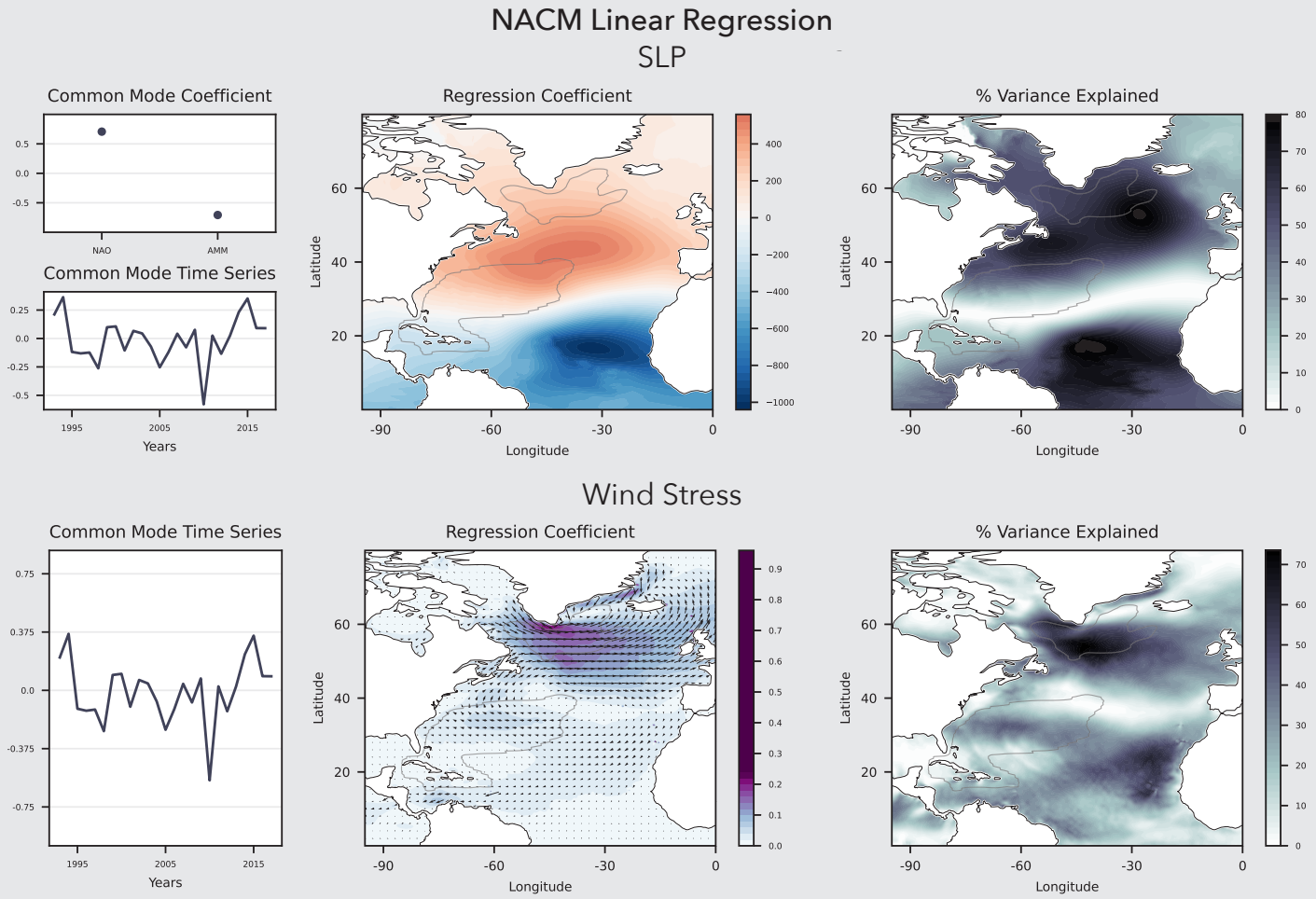

Figure 19 : Common Mode linear regression plots onto SLP and Wind Stress data. Spatial and temporal components of PC0 are in the left most column. Regression coefficient maps are in the center. Percent Variance explained is in the right most column.

3.3.2 The North Atlantic Common Mode

The NACM time series was derived from conducting SVD analysis on the NAO and AMM time series. The first component of this analysis explains 78.6% of the variance in both of these time series. This was labeled the NACM because it describes the time series that is shared between both modes of variability.

The linear regression plots of this mode onto SST, altimeter, SLP and wind stress fields are shown in Figures 18 and 19. In the left hand column of these figures are two plots that describe the NACM. The bottom plot represents the time series of the NACM, while the top plot describes the coefficients associated with this time series for each individual mode of variability. These regression maps look very similar to that produced by the NAO because the NAO has a positive NACM coefficient. Conversely, these plots look like the inverse of the maps produced by the AMM because it has a negative NACM coefficient.

The NACM will be used in the following sections to draw comparisons between the known modes of variability and the ASM.

3.3.1 Annual Split Mode

The linear regression of the ASM onto SSH, SST, SLP and wind stress fields are shown in Figure 20 and 21.

The SST and Altimeter linear regression coefficient plots illustrate a very similar tripole pattern. This tripole is defined by positive values in the high and low latitudes, and negative values in the mid latitudes.

The SST maps have a high variance explained value for large regions of the tripole shape. In contrast, the altimeter maps have a less consistent spatial pattern. Although both of these variables show consistent large values for variance explained along the SAB.

The change in sign of the regression coefficients along the coast across Cape Hatteras is consistent with our expectations as the time series being regressed is associated with a split at this location.

The wind stress linear regression maps illustrate a decrease of the westerlies located at higher latitudes, in addition to a slight decrease in the trade winds located at mid to low latitudes. This wind stress pattern also illustrates an increase in westerly winds between 30-40°N off of the US East Coast. These wind anomalies could be partially responsible for the SST and altimeter anomalies.

An increase in wind over the mid latitudes could result in increased THF leading to negative SST anomalies. Conversely, simultaneous decreases in prevailing winds over the high and low latitudes could result in decreased THF leading to positive SST anomalies. While

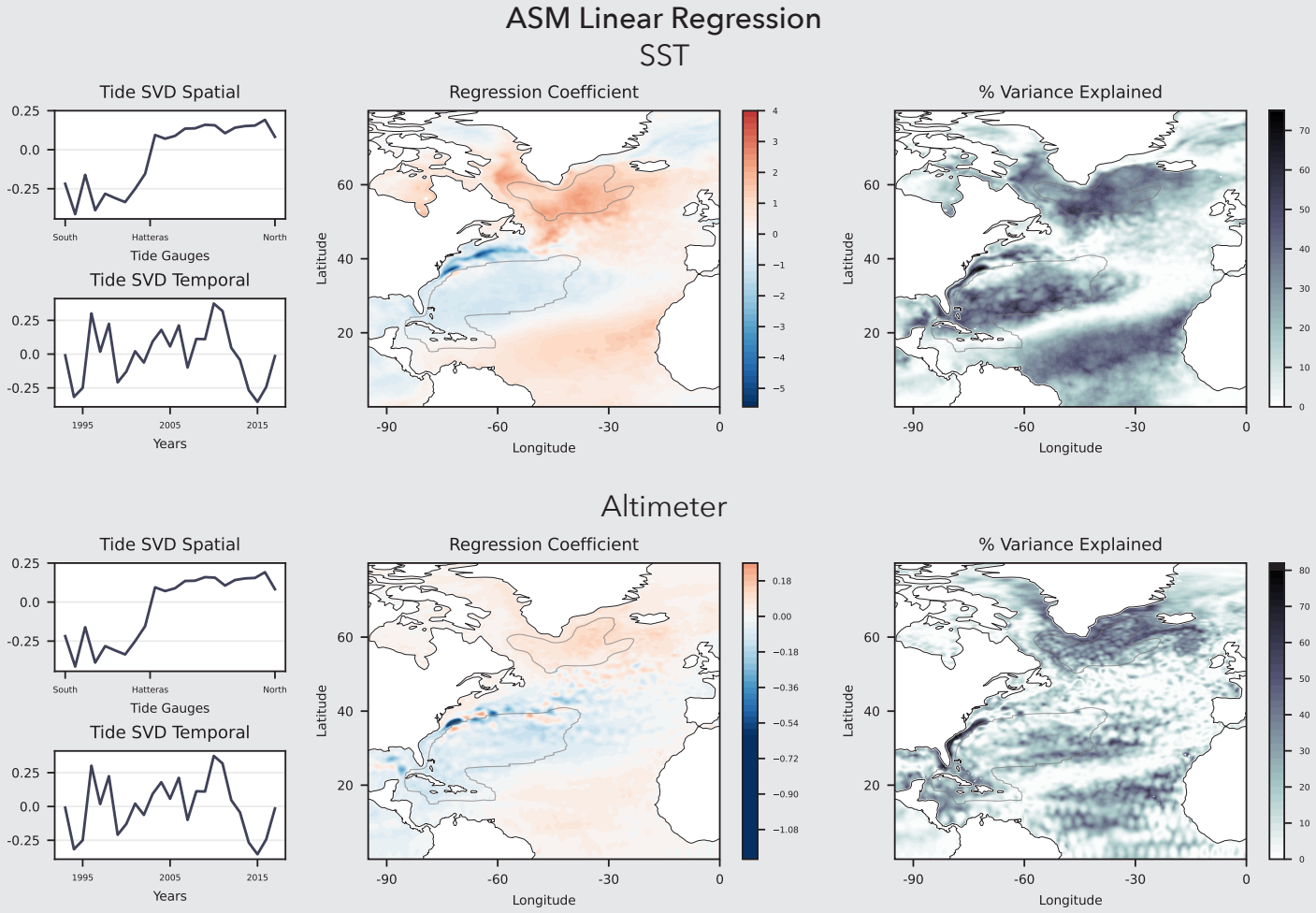

Figure 20 : Annual Split mode (PC0) linear regression plots onto SST and Altimeter data. Spatial and temporal components of PC0 are in the left most column. Regression coefficient maps are in the center. Percent Variance explained is in the right most column.

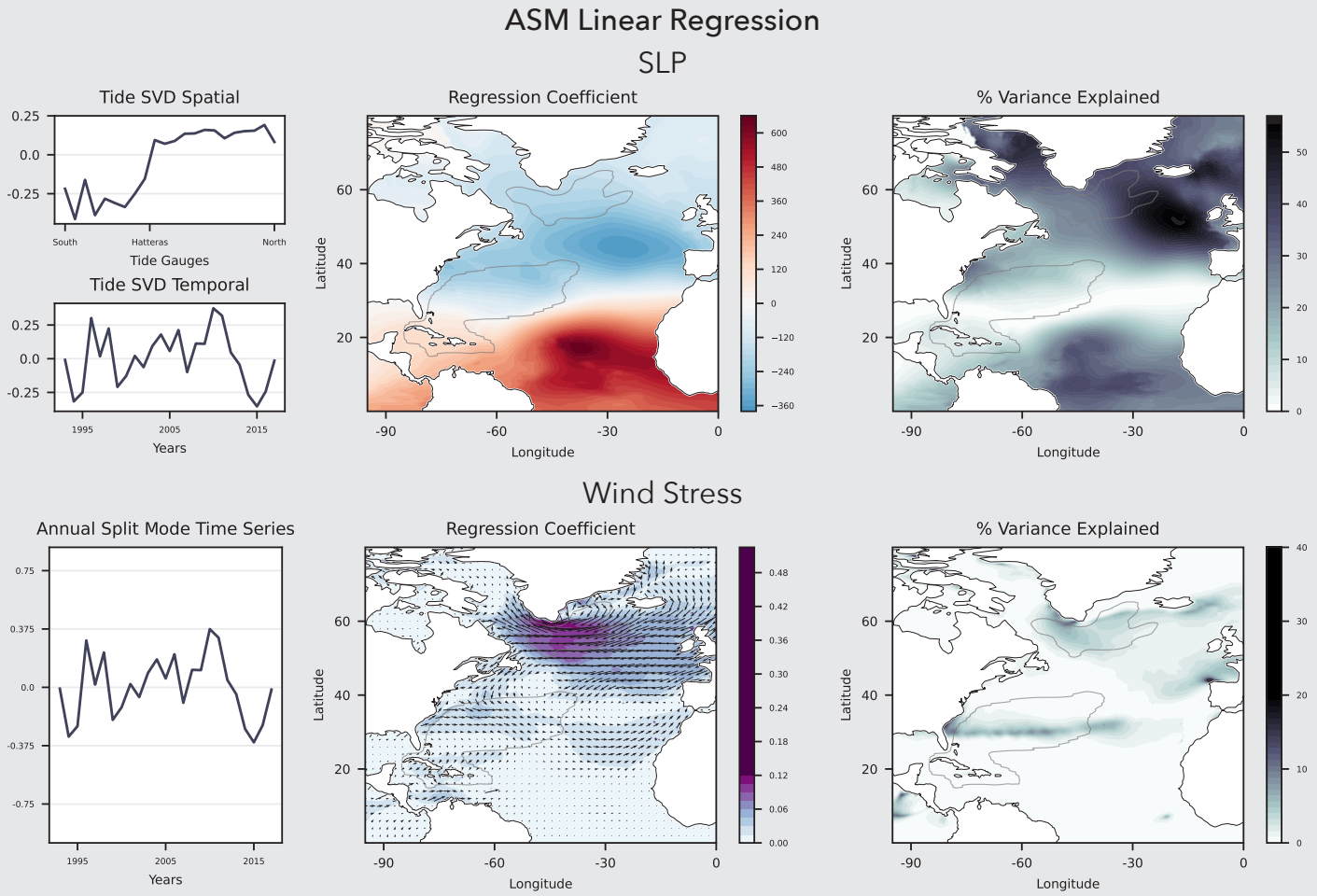

Figure 21 : Annual Split mode (PC0) linear regression plots onto SLP and Wind Stress data. Spatial and temporal components of PC0 are in the left most column. Regression coefficient maps are in the center. Percent Variance explained is in the right most column.

these wind stress anomalies may explain the SST tripole pattern, they don't explain the SSH pattern shown in the altimeter regression maps.

The wind stress anomalies that are consistent with a weakening of the westerlies and trade winds indicate that there may be related anomalies in gyre transport. This pattern of wind anomalies would be consistent with decreased subtropical gyre transport. If this is the driving mechanism behind the SSH tripole pattern, then we can infer that a decrease in subtropical gyre transport would lead to a decrease in SSH in the subtropical gyre region. This mechanism is further explored in Section 3.4.

The relationship between wind forcing and SSH is further complicated by the presence of along shore wind stress anomalies along the US East Coast.

Local vs Remote Wind Stress Forcing

The subpolar and subtropical gyres are predominantly driven by these prevailing wind patterns. Thus, a decrease in these patterns could be consistent with a decrease in the magnitude of gyre transport. Due to the geostrophic nature of gyre circulation, a decrease in overall transport of the subtropical gyre would be consistent with the decrease in SSH in the gyre region as depicted in the altimeter linear regression maps.

While this would explain the large scale pattern, it is possible that local wind stress plays a role in these SSH anomalies as well. The increased wind stress over the mid latitudes follows the coastline south of Cape Hatteras in the north east direction. A close up of this region is depicted in Figure 22.

This alongshore wind stress could indicate an increase in offshore Ekman Transport in the SAB and parts of the MAB. It is also notable that there are similar alongshore wind stress anomalies in the Gulf of Maine moving in the south west direction. This could drive an increase in onshore Ekman transport, contributing to the positive SSH anomaly present in this region.

The region of potential offshore Ekman transport located in the MAB raises the question of the role of local and remote wind stress forcing in driving US East Coast sea level variability. In the SAB and GOM, the potential Ekman transport and associated changes in coastal sea level coincide with changes in coastal sea level predicted from basin scale wind forcing and subsequent changes in gyre transport.

For example, the remote wind stress pattern is consistent with decreasing westerlies and trade winds. This would result in decreased subtropical gyre transport, and a decrease in SSH over the subtropical gyre region. At the same time, the alongshore wind stress in this region is consistent with offshore Ekman transport, leading to a compounded effect of decreased coastal sea level.

However, in the case of the MAB, these two forces do not coincide. The remote wind stress pattern is associated with an increase in coastal sea level in this region, while the alongshore wind stress is consistent with increased offshore Ekman transport and subsequent decreases in coastal sea level. Despite these competing mechanisms, the fact that this region is associated with increased sea level indicates that remote wind stress forcing plays a larger role in driving coastal sea level variability.

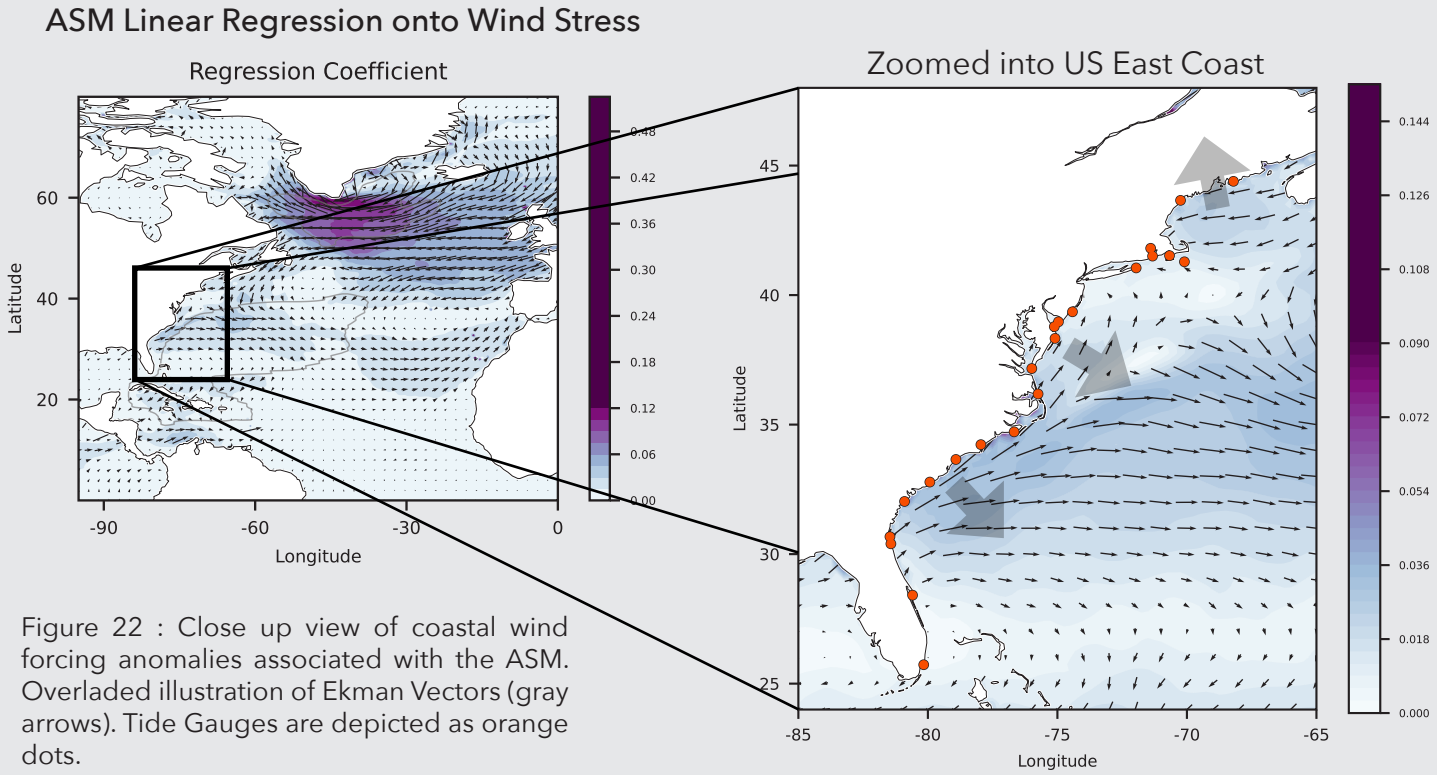

Figure 22 : Close up view of coastal wind forcing anomalies associated with the ASM. Overladed illustration of Ekman Vectors (gray arrows). Tide Gauges are depicted as orange dots.

3.4 Analysis of ECCO Data

The analysis of ECCO data is comprised of two primary sections: identifying the dominant modes of variability through the use of EOF analysis and exploring the expression of the NACM and ASM in ECCO data. The velocity field from ECCO provides the ability to regress these variables onto the barotropic streamfunction, enabling the exploration of gyre transport variability.

3.4.1 Dominant Modes of Variability within Wind Stress, SF and SSH Fields

The dominant modes of variability within each variable field were extracted through the use of EOF analysis. The time series associated with each PC were then correlated to tide gauge data. These are shown in Figures 23-26.

Wind

The wind stress field was passed into EOF analysis as complex values. The zonal component comprised the real component, while the meridional component comprised the imaginary component. This enabled the EOF analysis of the entire wind vector field. This resulted in one time series for each directional component of the vector field. While the zonal and meridional components are associated with different spatial and temporal patterns, they combine to produce the first mode of the wind stress vector field. Combined, they explain

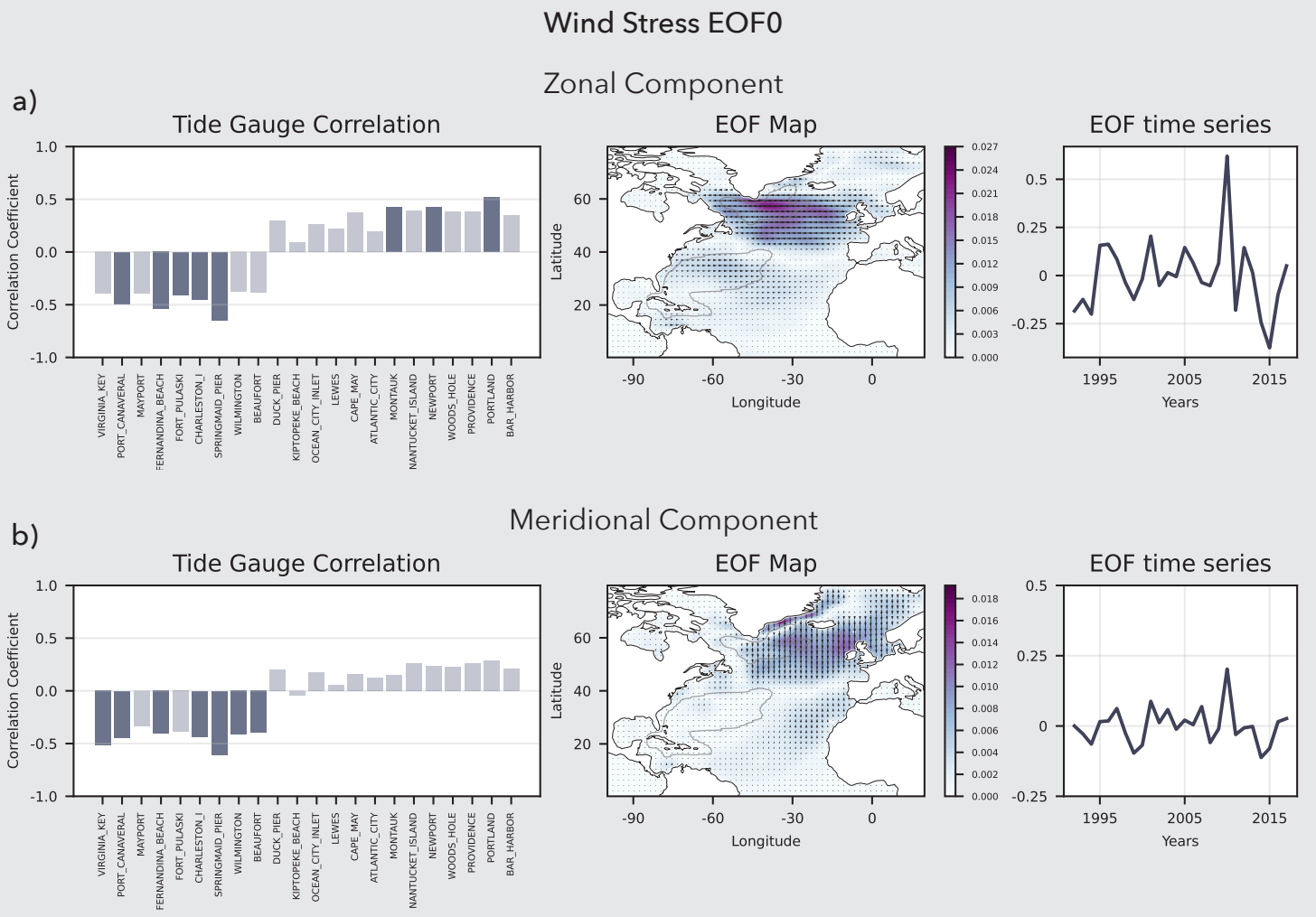

Figure 23 : These maps depict the zonal and meridional component of the wind stress vector field EOF0. The collectively account for 33% of the variance in this vector field. a) The zonal component of this EOF. b) The meridional component.

33% of the original vector field. The composite of the zonal and meridional components is referenced as EOF0, as they collectively are the first EOF of the wind stress field.

The correlation values of the tide gauges to the zonal and meridional components varies in magnitude and significance. The zonal component appears to be more significant for some of the tide gauges in the MAB and GOM. This is due to the fact that none of the correlation values between tide gauges in these regions and the meridional component of the wind vector EOF are significant at the 95th percentile. However, both the zonal and meridional time series result in significant correlations to tide gauges in the SAB. Between both correlation graphs, the sign of correlation with relationship to Cape Hatteras is consistent. Tide gauges in the SAB are negatively correlated to these wind stress anomalies, while tide gauges in the MAB and GOB are positively correlated.

Pictured in Figure 24 is the combination of zonal and meridional EOF spatial components. This wind field looks very similar to that of NACM and ASM. The wind stress anomalies around 40-60°N are consistent with a weakening of the westerlies, while the wind stress anomalies around 20-30°N are consistent with a weakening of the trade winds. Additionally, the narrow band of westerly anomalies around 30-40°N are also consistent with the regression maps

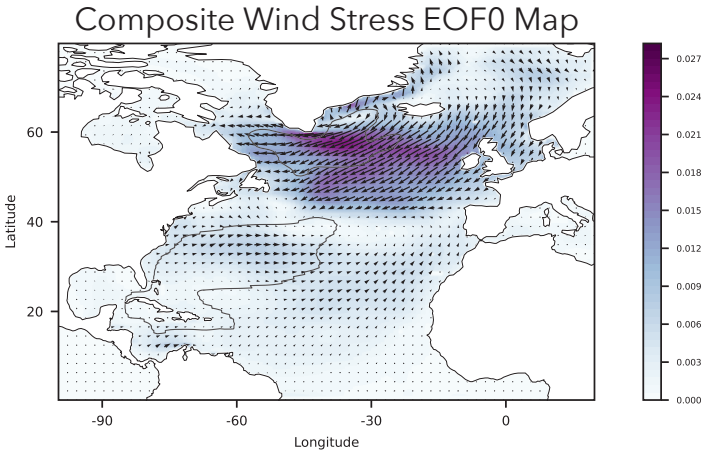

Figure 24 : This map depicts the combination of the zonal and meridional EOF0 components.

produced by the NACM and ASM.

Not only does the composite map of both zonal and meridional components of the EOF closely resemble the linear regression coefficient map produced by the ASM, their relationships to tide gauges along the US East Coast are also consistent. Tide gauges in the SAB are associated with a negative spatial coefficient for the ASM mode. Similarly, the correlation values between the SAB and wind stress EOF time series are also negative. Based on the EOF spatial pattern, this is what we expect.

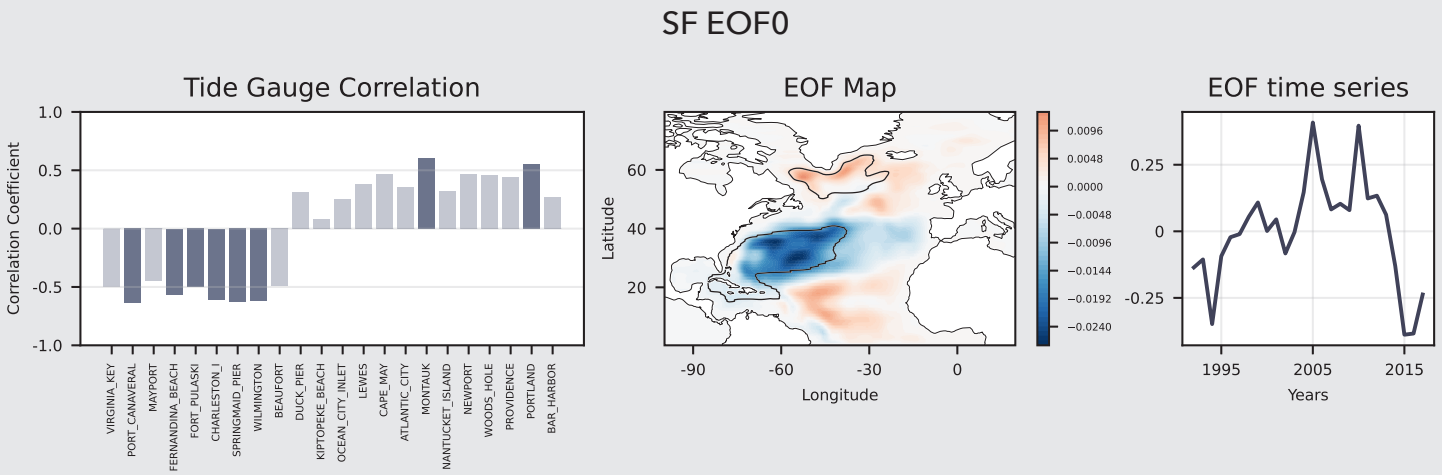

Figure 25 : SSH and Barotropic SF first EOF. Tide Gauge correlation is shown in the left column. EOF shown in the middle column. PC time series shown in the right column. Significant correlations at the 95th percentile are darker in color.

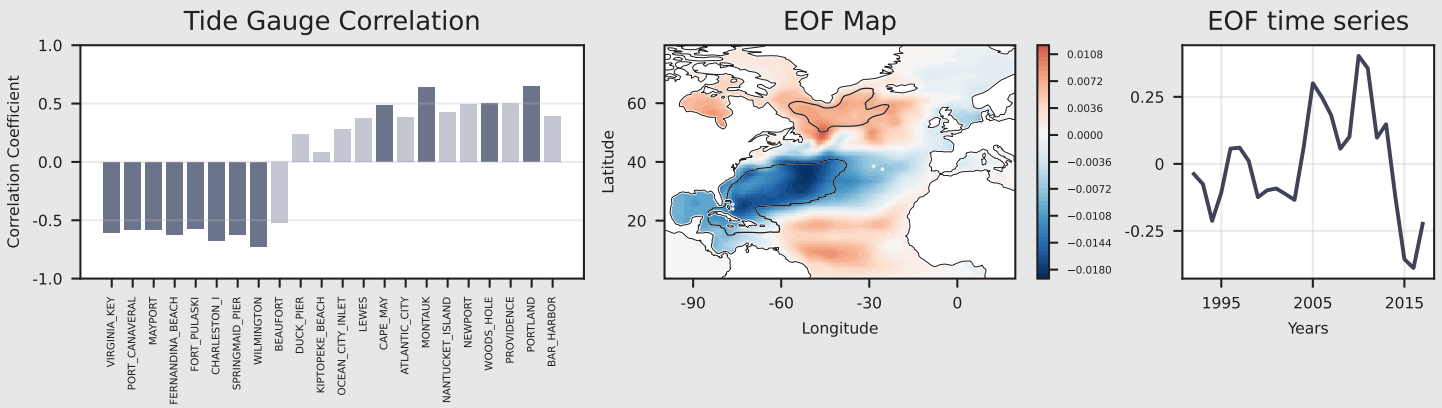

Figure 26 : Wind first EOF. Tide Gauge correlation is shown in the left column. EOF shown in the middle column. PC time seris shown in the right column. Significant correlations at the 95th percentile are darker in color.

Streamfunction

SF EOF0 depicts a positive relationship between the subpolar gyre transport and the region between 0-20°N. These two regions are also shown to be inversely related to the subtropical gyre region. However, since the subpolar gyre is typically associated with a negative value, a positive anomaly would indicate a decrease in gyre transport. Similarly, since the subtropical gyre transport is typically associated with a positive value, a negative anomaly would also indicate a decrease in transport. Thus, this dominant mode of variability, accounting for 31% of the overall variability in the SF field, can be interpreted as representing a simultaneous weakening (strengthening) of both gyres during periods of negative (positive) time series values.

The time series associated with this simultaneous increase in gyre transport is negatively correlated to tide gauges in the SAB, and positively correlated to tide gauges in the MAB and GOM. From this information, we can infer that when the subtropical gyre experiences a decrease in gyre transport, sea level along the coast of the SAB also decreases, while sea level in the MAB and GOM increases. This change in correlation sign across Cape Hatteras indicates that SF EOF0 may play a crucial role in the ASM.

Sea Surface Height

SSH EOF0 has a very similar spatial pattern and time series to that of SF EOF0. The high and low latitudes are positively correlated, and inversely correlated to the mid latitudes. The tide gauge correlation graph also has a very similar shape. Tide gauges in the SAB are negatively correlated to this time series, which indicates that they are positively correlated to the subtropical gyre region. On the other hand, the tide gauges in the MAB and GOM are positively correlated to the time series, indicating that they are positively correlated to the subpolar gyre region.

Relationship Between Wind, SF & SSH

The wind stress EOF0 and the SF EOF0 have correlation values of 0.64 ($p = 0.004$) for the zonal component, and 0.40 ($p = 0.040$) for the meridional component. These values indicate that the dominant mode of wind stress variability is significantly related to the dominant mode of SF variability.

The SF EOF0 and the SSH EOF0 time series have a correlation value of 0.88 ($p = 0.004$). This indicates that there is a very close relationship between SF anomalies and SSH anomalies. For the subtropical gyre region, this indicates that when the SF decreases, SSH decreases. For the subpolar gyre region, this indicates that when the SF decreases, SSH increases.

3.4.2 Basin Scale Expression of the ASM

The same linear regression techniques described in previous sections were applied to ECCO data. The results are shown in Figures 27 and 28.

The regression coefficient plot of the ASM onto the wind stress field is consistent with the regression maps produced in previous sections. In previous sections, the relationship between wind stress anomalies that indicate a weakening of the westerlies and trade winds in addition to potential changes in gyre transport are confirmed by the SF regression map. A simultaneous weakening of prevailing winds coincides with a decrease in gyre transport for the subtropical gyre. Additionally, the positive SF anomaly along the western boundary of the subtropical gyre may be a result of the alongshore wind stress anomalies in this region.

The map of SSH linear regression coefficients displays a negative SSH anomaly over the entire mid latitudes. This indicates that both the positive and negative SF anomalies in this region contribute to decreasing SSH. It is possible that the majority of this decrease in SSH is related to the negative streamfunction anomalies, while the positive anomaly is responsible for the decrease in SSH along the coast in the SAB.

From our physical understanding of the subtropical gyre, we know that the geostrophic currents that comprise gyre transport are in the same direction as the original wind stress. Additionally, an increase in geostrophic currents would dictate an increase in Ekman transport

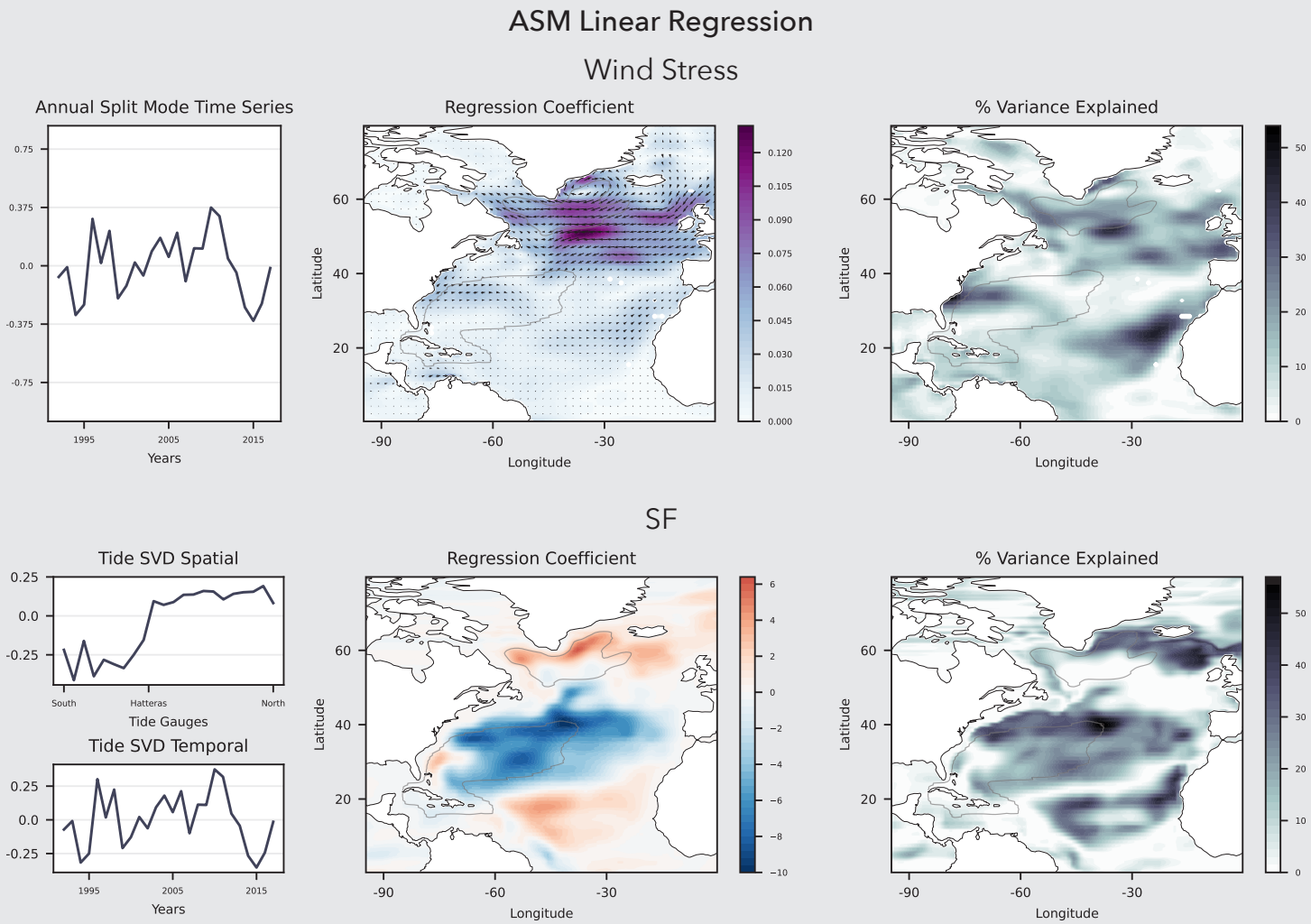

Figure 27 : Annual Split mode Linear Regression maps for Wind stress and Barotropic streamfunction. The annual split mode time series is shown in the left column. A map of the regression coefficients are shown in the middle column. Percent Variance explained maps are shown in the right most column.

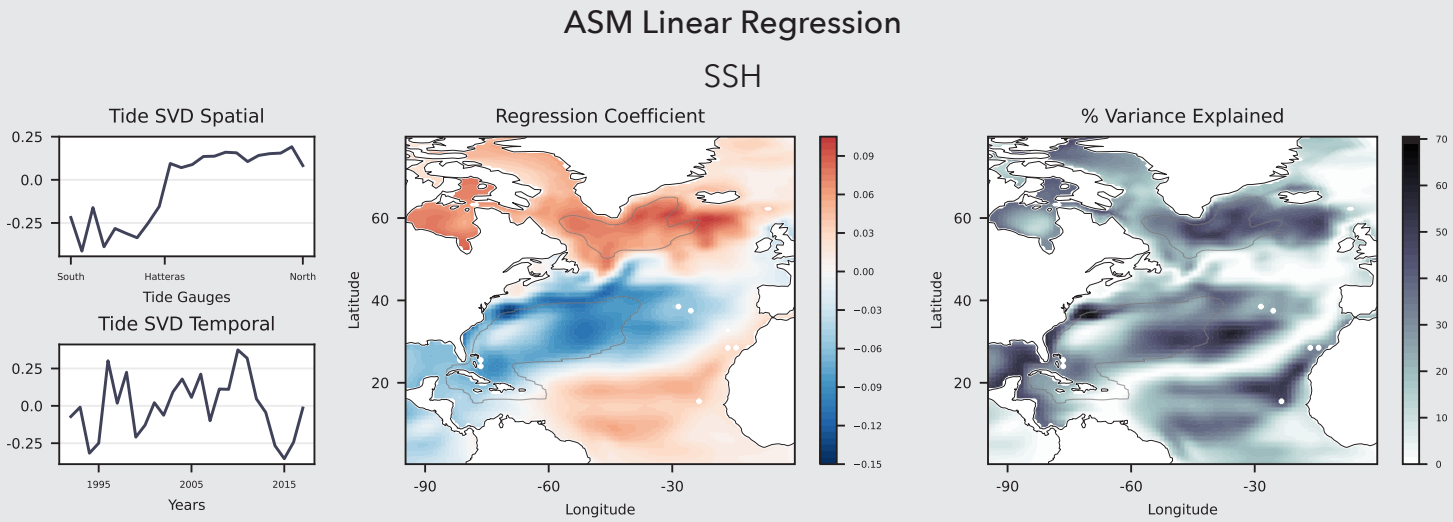

Figure 28 : Annual Split mode linear regression map for SSH. Split mode time series is shown in the left column. A map of regression coefficients is shown in the center. Percent variance explained is shown in the right column.

toward the center of the gyre. This would result in offshore Ekman transport, leading to the negative SSH anomalies along the coast of the SAB.

3.4.3 Basin Scale Expression of the NACM

The linear regression maps of the NACM onto wind stress reveals a similar pattern to that of the ASM. These two time series have a correlation value of -0.72 (p = 3.5e-5), resulting in an inverse of the regression coefficient maps between these two modes. Accounting for this inverse, one large difference between the wind stress regression coefficient map of the NACM and the ASM, is the lack of alongshore wind stress for the NACM. For the NACM, the wind stress anomalies in the mid latitudes span a wider range of latitudes, and extend more uniformly to the center of the North Atlantic. However, as these wind anomalies approach the coast, they do not turn toward the south west to run alongshore.

This difference in wind anomalies may result in the differences present in the SF map.

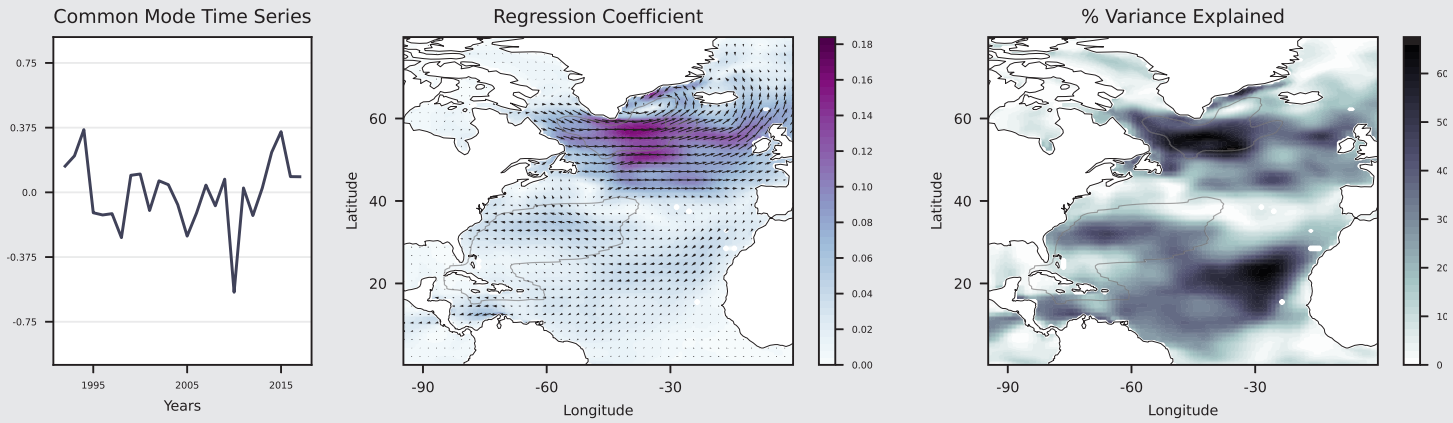

Figure 29 :Common Mode linear regression map for wind stress. The common time series is shown in the left. A map of the regression coefficients is shown in the center. Percent variance explained is shown on the right.

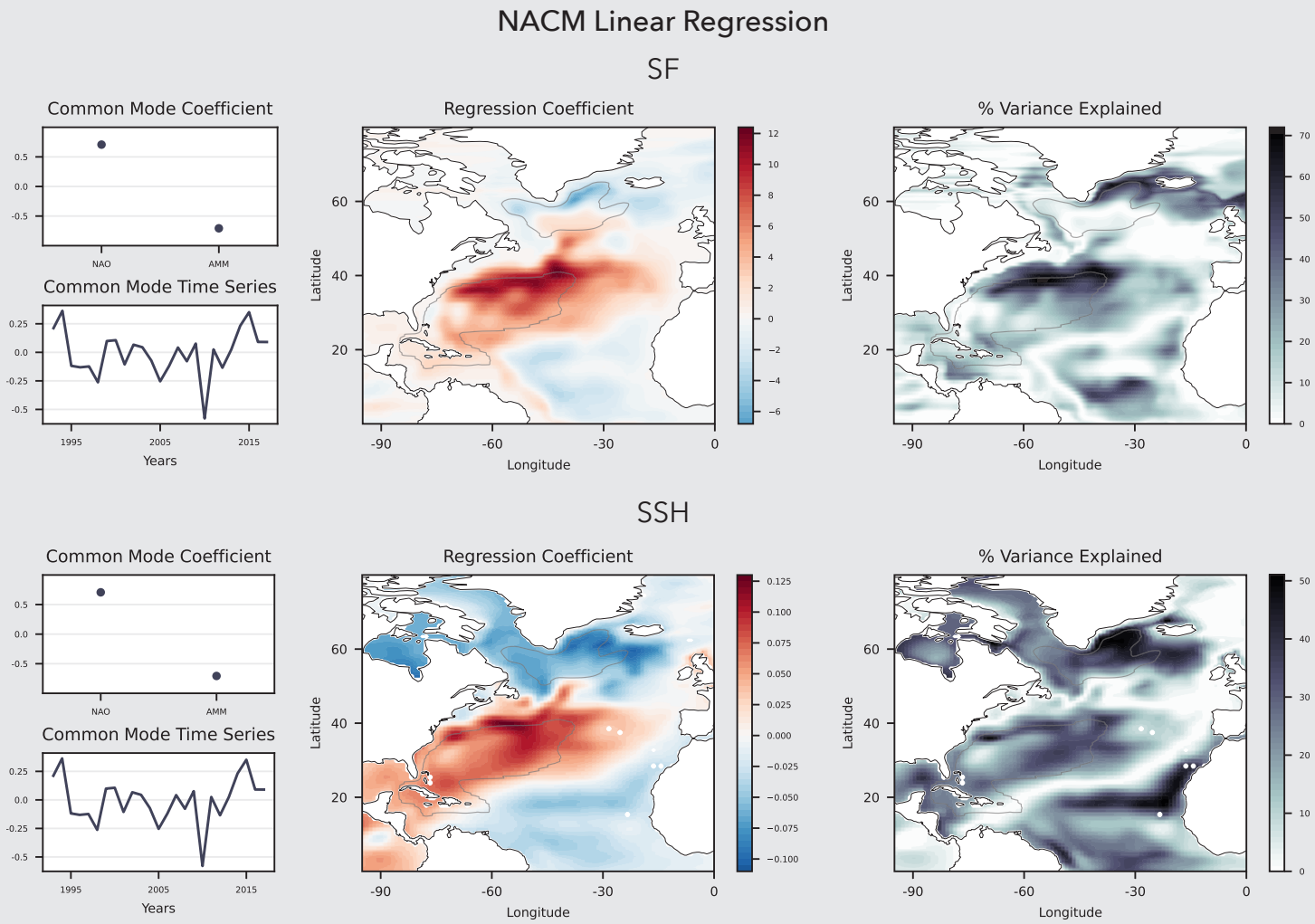

Figure 30 : Common mode regression maps for Barotropic Streamfunction and SSH. The common mode time series is shown in the left column. Maps of regression coefficients are shown in the middle column. Percent variance explained is shown in the right column.

The SF regression coefficient map looks very similar to that of the ASM. The magnitude of the SF regression coefficient across the majority of the mid latitudes is approximately the same between both modes. However, the magnitude of the regression coefficient at the western boundary is much smaller.

The smaller difference between the majority and the western boundary of the subtropical gyre region may be the cause of the more uniform SSH regression coefficients over this region, and the slightly smaller coefficient magnitude along the coast of the SAB.

4. Discussion

4.1 RAPID Ekman wind Pattern and Atmospheric Modes of Variability

The RAPID Ekman time series linearly regressed onto the ERA5 wind stress field produced a regression coefficient map that is very similar to that of the NACM. Because the RAPID Ekman time series is the estimated northerly Ekman transport resulting from zonal wind stress along 26.5°N, once detrended it should look very similar to a time series of the anomalous zonal wind stress in this region. As such, it makes sense that this regression map looks very similar to that of the NACM as this is representative of both of the dominant modes of variability in the North Atlantic.

From the NACM regression maps of SSH, and the correlation value between the NACM and the ASM, the split in correlation sign across Cape Hatteras is in agreement with our expectations.

4.2 ECCO EOF, ASM and NACM

The correlation values between the ECCO EOFs, ASM and the Atlantic modes of variability (AMM, NAO and NACM) are shown in Table 1.

The percent variance of the ECCO EOFs explained by the NACM are all around 50% with the exception of wind EOF0 where it explains 75% of the zonal and 47% of the meridional variability. This indicates that the NACM plays a large role in the tripole pattern present in both the SF and SSH EOFs. However, this also implies that there is a large fraction of variability that is not explained by the NACM.

The percent of ASM variance explained by the NACM is also around 50%. This indicates that the NACM plays a large role in the inverse relationship between sea level correlation across Cape Hatteras. However, the remaining signal is not so easily attributed to a single mode of climate variability. Regression maps of the residual ASM after removing the effect of the NACM are shown in Appendix 8.4.

4.3 Relationships Between Wind Stress and Sverdrup SF

Wind stress is the primary driver of gyre transport. We know this from the mechanistic understanding of gyre development. This section will use the Sverdrup streamfunction metric to solidify the understanding of the connection between changes in wind stress and changes in gyre transport.

Figure 31 includes the coefficient map of the NACM linearly regressed onto wind stress, the Sverdrup SF calculated from this wind stress field, and the coefficient map of the NACM linearly regressed onto the barotropic SF field. As stated in previous sections, the wind

	Wind EOF0	SF EOF0	SSH EOF0	ASM
AMM	(0.71, 0.61)	0.74	0.67	0.64
NAO	(-0.82, -0.60)	-0.62	-0.53	-0.63
NACM	(-0.87, -0.67)	-0.77	-0.67	-0.72
% Variance Explained by the NACM	(75%, 47%)	59%	45%	52%

Table 1. All Rows 1-3 are correlation values significant at the 95th percentile. Row 4 is the variance of each column's variable that is explained by the NACM

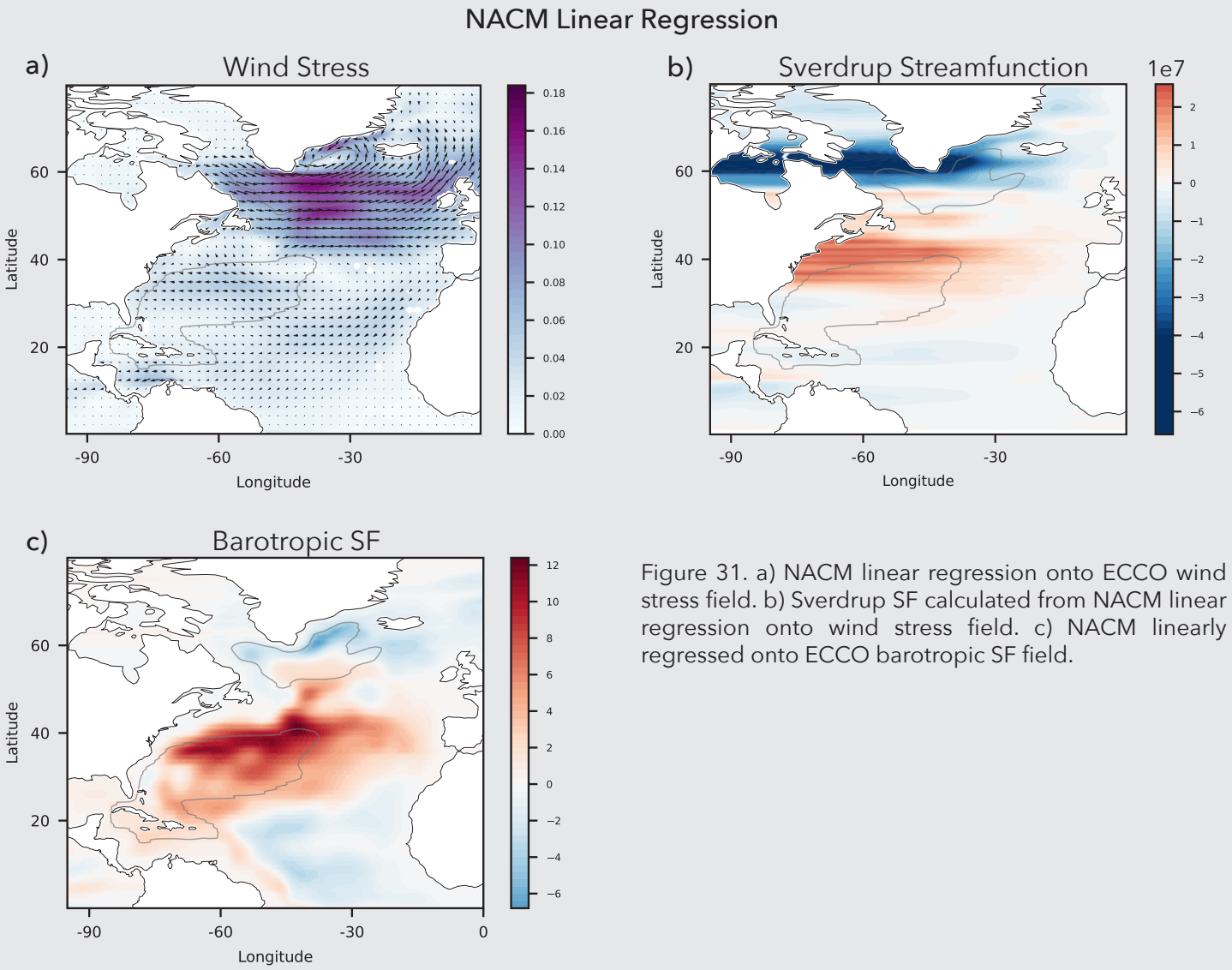

Figure 31. a) NACM linear regression onto ECCO wind stress field. b) Sverdrup SF calculated from NACM linear regression onto wind stress field. c) NACM linearly regressed onto ECCO barotropic SF field.

stress regression coefficient map depicts wind anomalies consistent with a strengthening of the westerlies and trade winds. The Sverdrup SF is then calculated by computing the curl of this wind stress anomaly field, and then zonally integrating this field from east to west.

The Sverdrup SF plot depicts an increase in gyre transport along the northern edge of the gyre, in addition to a smaller increase along the eastern edge, extending down to around 20°N. This spatial pattern is consistent with the increased gyre transport depicted in the barotropic SF regression coefficient map.

Interestingly, the Sverdrup SF also predicts a decrease in gyre transport near the center of the gyre region, and extending toward the west. This negative anomaly also shows up in the barotropic SF regression coefficient map. This confirms that the changes in the barotropic SF field are consistent with changes in the prevailing wind stress patterns depicted in the wind stress regression coefficient map.

4.4 Conclusions

The culmination of the analysis conducted throughout this thesis reveals a potential mechanistic description of the influence of the SST and SSH tripole patterns on coastal sea level variability.

As confirmed in the previous section, wind is the driver of the basin-scale sea level variations and the observed coastal sea level variations. On a basin scale, the observed wind anomalies affect SST in two ways: through changes in turbulent heat fluxes, and through

changes in gyre transport. This change in gyre transport may be responsible for changes in heat divergence associated with the NAO that has been highlighted in previous work (Volkov et al., 2019). On the other hand, SSH is associated with changes in gyre transport in response to changes in prevailing wind stress patterns.

On a local scale, changes in SSH along the US East Coast are driven by both local and remote wind forcing. While both of these are present in our analysis of one of the leading modes of annual sea level variability, it can be concluded that the changes in basin scale gyre transport dominate over localized wind anomalies along the coast.

The shared component of variability between the NAO and AMM is responsible for 52% of the variability that drives the inverse correlation of tide gauges across Cape Hatteras. The basin scale expression of this mode of variability results in changes in coastal sea level. Moreover, changes in gyre transport have a substantial effect on coastal sea level.

This thesis highlights the contribution of the NAO and AMM in the dominant modes of wind stress, SF and SSH variability. However, the residual variance certainly implies that there are other substantial driving factors that result in a tripole-like pattern of sea level and gyre variability. Additionally, future work should focus on the substantial fraction (nearly 50%) of the variance of the annual mode of variability that is anticorrelated across Cape Hatteras not explained by the NAO and AMM (see Section 7.2).

Wind-driven basin-scale dynamics across the entire North Atlantic drive changes in coastal sea level along the US East Coast. The effects of this interannual variability alternate sign across Cape Hatteras. The results of this thesis indicate that future changes in basin-scale dynamics can have spatially complex effects on coastal sea level.

5. Acknowledgments

Kris Karnauskas as been an amazing advisor throughout this entire project. At first, when we were discussing the potential of this project and realized we were short on time, he took a chance on me and believed in my determination. Truthfully, determination was about all I had at that point. He was incredibly patient and supportive throughout this entire project. This was especially true at the beginning, when I started to realize how different research is from coursework and how much more I needed to learn. He has continued to provide an ideal balance of supporting guidance and independence. I could not have asked for a better advisor or introduction to research.

Chris Little has also been invaluable to this project. He was visiting Boulder when this project began, and has continued to provide his advice and knowledge remotely. His unexpected and interesting insights always keep our meetings lively, and his broad expertise and knowledge of the field help guide me at every turn.

This thesis would not be what it is today without either of them. I am grateful for both Kris and Chris, and hope they will continue to advise me throughout my career.

Derek Brown has been essential in laying the groundwork for this project. He guided me through the Honors Thesis process and has helped keep me on track. I'd also like to thank him for serving on my committee, and being the bridge between ATOC and the Honors Council.

Finally, I'd also like to thank Steve Nerem for serving on my committee, and making time during such a busy part of the semester.

6. References

Andres, M. (2021). Spatial and temporal variability of the Gulf Stream near Cape Hatteras. *Journal of Geophysical Research: Oceans*, 126, e2021JC017579. https://doi.org/10.1029/2021JC017579

Bingham, R. J. & Hughes, C. W. Signature of the Atlantic meridional overturning circulation in sea level along the east coast of North America. *Geophys. Res. Lett*. 36, (2009).

Cayan, D. R., 1992: Latent and sensible heat flux anomalies over the northern oceans: Driving the sea surface temperature. *J. Phys. Oceanogr.*, 22, 859–881.

Dangendorf, S., Hendricks, N., Sun, Q. et al. Acceleration of U.S. Southeast and Gulf coast sea-level rise amplified by internal climate variability. *Nat Commun* 14, 1935 (2023). https://doi.org/10.1038/s41467-023-37649-9

Diabaté, S. T., Swingedouw, D., Hirschi, J. J.-M., Duchez, A., Leadbitter, P. J., Haigh, I. D., and McCarthy, G. D.: Western boundary circulation and coastal sea-level variability in Northern Hemisphere oceans, *Ocean Sci.*, 17, 1449–1471, https://doi.org/10.5194/os-17-1449-2021, 2021.

Frajka-Williams, E., Meinen, C. S., Johns, W. E., Smeed, D. A., Duchez, A., Lawrence, A. J., Cuthbertson, D. A., McCarthy, G. D., Bryden, H. L., Baringer, M. O., Moat, B. I., and Rayner, D.: Compensation between meridional flow components of the Atlantic MOC at 26° N, *Ocean Sci.*, 12, 481–493, https://doi.org/10.5194/os-12-481-2016, 2016.

Frankignoul, C., 1985: Sea surface temperature anomalies, planetary waves and air-sea feedback in the middle latitudes. *Rev. Geo-phys.*, 23, 357–390.

Hátún, H., & Chafik, L. (2018). On the recent ambiguity of the North Atlantic subpolar gyre index. *Journal of Geophysical Research: Oceans*, 123, 5072–5076. https://doi.org/10.1029/ 2018JC014101

Holgate, S.J.; Matthews, A.; Woodworth, P.L.; Rickards, L.J.; Tamisiea, M.E.; Bradshaw, E.; Foden, P.R.; Gordon, K.M.; Jevrejeva, S., and Pugh, J., 2013. New data systems and products at the Permanent Service for Mean Sea Level. *Journal of Coastal Research*, 29(3), 493–504. Coconut Creek (Florida), ISSN 0749-0208.

Jing, Y., Li, Y., and Xu, Y.: Assessment of responses of North Atlantic winter sea surface temperature to the North Atlantic Oscillation on an interannual scale in 13 CMIP5 models, Ocean Sci., 16, 1509–1527, https://doi.org/10.5194/os-16-1509-2020, 2020.

Karnauskas, K., Physical Oceanography and Climate, Cambridge University Press, 2020.

Little, C. M., Hu, A., Hughes, C. W., McCarthy, G. D., Piecuch, C. G., Ponte, R. M., & Thomas, M. D. (2019). The Relationship between U.S. East Coast sea level and the Atlantic Meridional Overturning Circulation: A review. *Journal of Geophysical Research*: Oceans, 124, 6435–6458. https://doi. org/10.1029/2019JC015152

Lohmann, K., Drange, H. & Bentsen, M. Response of the North Atlantic subpolar gyre to persistent North Atlantic oscillation like forcing. *Clim Dyn* 32, 273–285 (2009). https://doi.org/10.1007/s00382-008-0467-6

Moat, B. I., Smeed, D. A., Frajka-Williams, E., Desbruyères, D. G., Beaulieu, C., Johns, W. E., Rayner, D., Sanchez-Franks, A., Baringer, M. O., Volkov, D., Jackson, L. C., and Bryden, H. L.: Pending recovery in the strength of the meridional overturning circulation at 26° N, *Ocean Sci.*, 16, 863–874, https://doi.org/10.5194/os-16-863-2020, 2020.

Park, J. and Sweet, W.: Accelerated sea level rise and Florida Current transport, *Ocean Sci.*, 11, 607–615, https://doi.org/10.5194/os-11-607-2015, 2015.

Piecuch, C. G., & Beal, L. M. (2023). Robust weakening of the Gulf Stream during the past four decades observed in the Florida Straits. *Geophysical Research Letters*, 50, e2023GL105170. https://doi.org/10.1029/2023GL105170

Piecuch, C. G., Dangendorf, S., Gawarkiewicz, G. G., Little, C. M., Ponte, R. M., & Yang, J. (2019). How is New England coastal sea level related to the Atlantic meridional overturning circulation at 26°N? *Geophysical Research Letters*, 46, 5351-5360. https://doi.org/10.1029/2019GL083073

Polo, I., J. Robson, R. Sutton, and M. A. Balmaseda, 2014: The Importance of Wind and Buoyancy Forcing for the Boundary Density Variations and the Geostrophic Component of the AMOC at 26°N. *J. Phys. Oceanogr.*, 44, 2387–2408, https://doi.org/10.1175/JPO-D-13-0264.1.

Seip, Knut Lehre, Øyvind Grøn, and Hui Wang. 2019. "The North Atlantic Oscillations: Cycle Times for the NAO, the AMO and the AMOC" Climate 7, no. 3: 43. https://doi.org/10.3390/cli7030043

Smeed, D. A., Josey, S. A., Beaulieu, C., Johns, W. E., Moat, B. I., Frajka-Williams, E., et al. (2018). The North Atlantic Ocean is in a state of reduced overturning. *Geophysical Research Letters*, 45, 1527–1533. https://doi.org/10.1002/ 2017GL076350

Valle-Levinson, A., A. Dutton, and J. B. Martin (2017), Spatial and temporal variability of sea level rise hot spots over the eastern United States, *Geophys. Res. Lett.*, 44, 7876–7882, doi:10.1002/ 2017GL073926.

Volkov, D. L., Lee, S.-K., Domingues, R., Zhang, H., & Goes, M. (2019). Interannual sea level variability along the southeastern seaboard of the United States in relation to the gyre-scale heat divergence in the North Atlantic. *Geophysical Research Letters*, 46, 7481–7490. https://doi.org/10.1029/ 2019GL083596

Walker, G. T.: Correlation in seasonal variations of weather-A fur- ther study of world weather, Mon. Weather Rev., 53, 252–254, 1924.

Wang, W., B. T. Anderson, R. K. Kaufmann, and R. B. Myneni, 2004: The Relation between the North Atlantic Oscillation and SSTs in the North Atlantic Basin. *J. Climate*, 17, 4752–4759, https://doi.org/10.1175/JCLI-3186.1.

https://www.aoml.noaa.gov/phod/research/tav/tcv/amm/index.php

Datasets:

Holgate, S.J.; Matthews, A.; Woodworth, P.L.; Rickards, L.J.; Tamisiea, M.E.; Bradshaw, E.; Foden, P.R.; Gordon, K.M.; Jevrejeva, S., and Pugh, J., 2013. New data systems and products at the Permanent Service for Mean Sea Level. *Journal of Coastal Research*, 29, 493–504. https://doi.org/10.2112/JCOASTRES-D-12-00175.1

https://rapid.ac.uk/index.php

Fukumori, I. (2022). Adjoint Modeling: A Brief Introduction (Version 2). Zenodo. https://doi.org/10.5281/zenodo.6080585

https://www.ncei.noaa.gov/products/optimum-interpolation-sst

https://www.ecmwf.int/en/forecasts/dataset/ecmwf-reanalysis-v5

https://podaac.jpl.nasa.gov/dataset/SEA_SURFACE_HEIGHT_ALT_GRIDS_L4_2SATS_5DAY_6THDEG_V_JPL2205

https://psl.noaa.gov/data/climateindices/

7. Appendices

7.1 Tide Gauge Selection

The bar graph shown below describes the relationships between all 43 tide gauges, their nearest altimeter cell, and their nearest ECCO grid cell. Opaque bars represent correlation values significant at the 95th percentile. The left most bar for each tide gauge describes the correlation value between the tide gauge and its nearest altimeter grid cell. This is used to assess the accuracy of the tide gauge data. The right most bar for each tide gauge describes the correlation between the tide gauge's nearest ECCO grid cell, and the altimeter grid cell at that location. This is used to gauge the accuracy of ECCO. Finally, the middle bar for each tide gauge represents the correlation between the altimeter grid cell at the coast, and the altimeter grid cell at the location of the nearest ECCO grid cell. This is used to understand the relationship between coastal and open ocean waters.

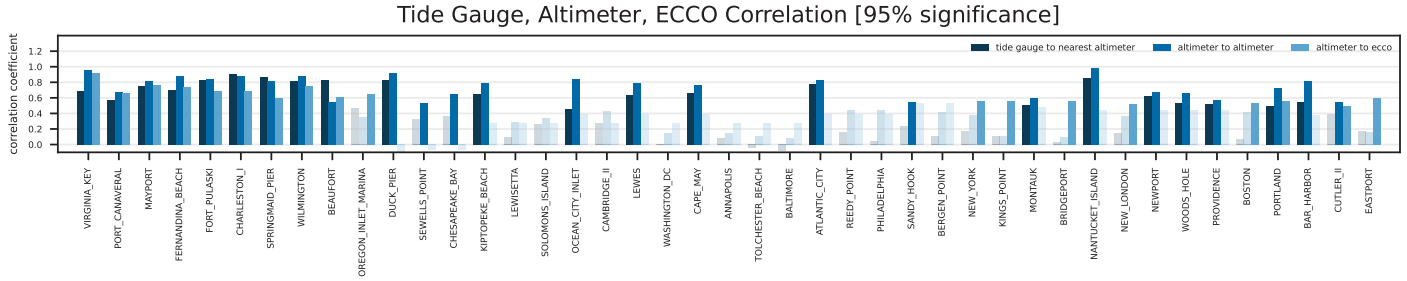

7.2 Residual ASM After Removing the NACM

The figures below depict the ASM after removing the variance explained by the NACM. This residual time series is then regressed onto SST, SSH, SLP and wind stress data to produce the following plots.

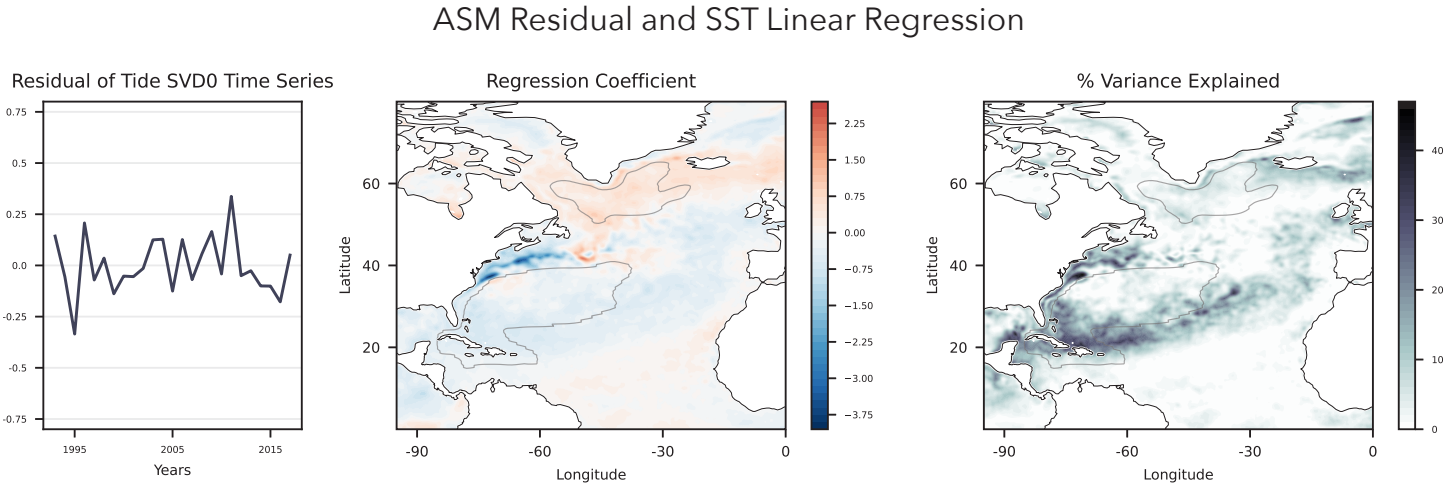

ASM Residual and SSH Linear Regression

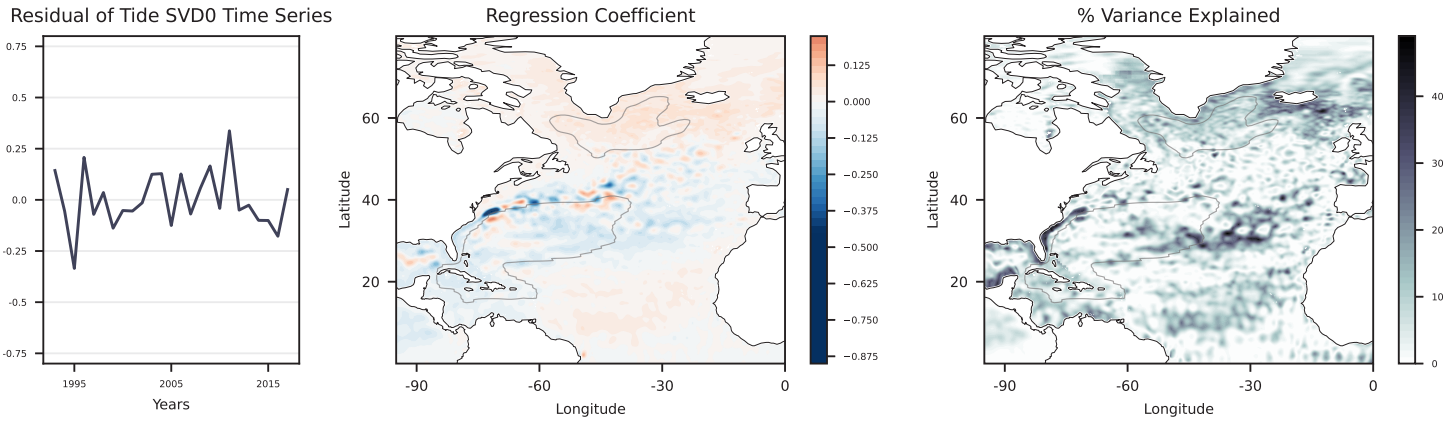

ASM Residual and SLP Linear Regression

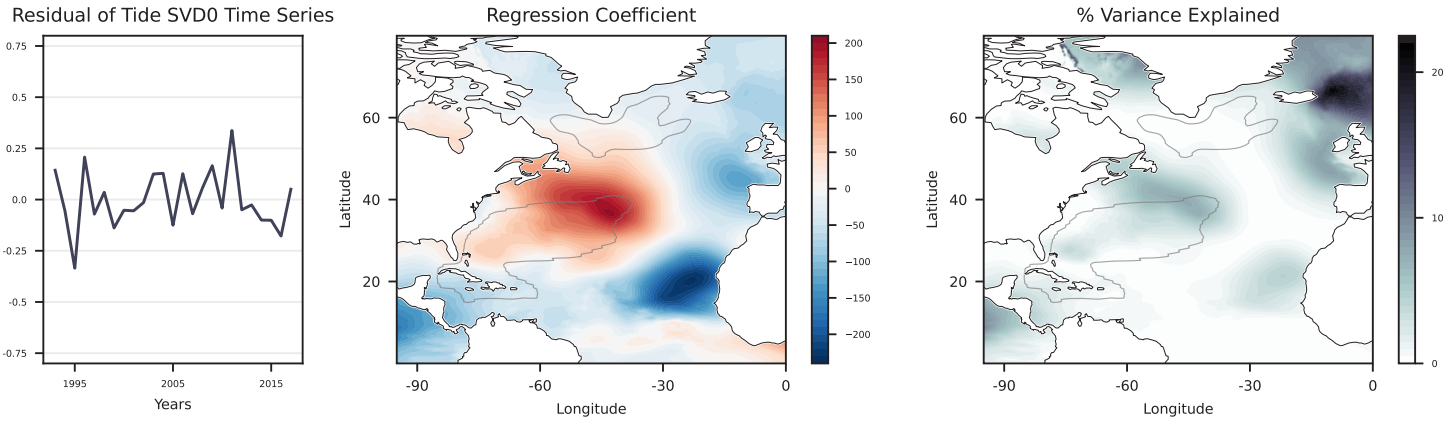

ASM Residual and Wind Stress Linear Regression